Research Square

Preprints are preliminary reports that have not undergone peer review.
They should not be considered conclusive, used to inform clinical practice,
or referenced by the media as validated information.

Mammalian Hemopexin Protects Blood-Feeding Dipterans from Heme Toxicity and Promotes Parasite Transmission

Joel Vega-Rodríguez

joel.vega-rodriguez@nih.gov

National Institute of Allergy and Infectious Diseases https://orcid.org/0000-0002-9576-0058

Francis de Souza Saraiva

National Institute of Allergy and Infectious Diseases

Thiago Alves e Silva

Johns Hopkins University https://orcid.org/0000-0002-8520-5405

Octavio Talyuli da Cunha

National Institute of Allergy and Infectious Diseases https://orcid.org/0000-0002-7026-463X

Eva Iniguez

Vector Molecular Biology Section, Laboratory of Malaria and Vector Research, National Institute of Allergy and Infectious Diseases, National Institutes of Health

Patricia Alvarenga

National Institute of Allergy and Infectious Diseases

Ana Barletta

National Institutes of Health https://orcid.org/0000-0001-9913-3775

Heather Kudyba

National Institute of Allergy and Infectious Diseases

Mahnaz Minai

NIAID, NIH

Motoshi Suzuki

National Institutes of Health https://orcid.org/0000-0002-4346-7677

Emanuela Tolosano

Molecular Biotechnology Center (MBC) Guido Tarone, Department of Molecular Biotechnology and Health Sciences, University of Torino https://orcid.org/0000-0002-1622-2340

Derron Alves

National Institutes of Health, USA

Jesus Valenzuela

National Institute of Allergy and Infectious Diseases https://orcid.org/0000-0002-5589-9450

Carolina Barillas-Mury

National Institutes of Health https://orcid.org/0000-0002-4039-6199

Shaden Kamhawi

National Institute of Allergy and Infectious Diseases https://orcid.org/0000-0003-4304-636X

Article

Keywords:

Posted Date: October 23rd, 2026

DOI: https://doi.org/10.21203/rs.3.rs-10295862/v1

License: This work is licensed under a Creative Commons Attribution 4.0 International License.
Read Full License

Additional Declarations: There is **NO** Competing Interest.

Mammalian Hemopexin Protects Blood-Feeding Dipterans from Heme Toxicity and Promotes Parasite Transmission

Francis M. de Souza Saraiva[1#], Thiago L. Alves e Silva[1], Octavio Talyuli da Cunha[1], Eva Iniguez[1], Patricia Hessab Alvarenga[1], Ana Beatriz Barletta Ferreira[1], Heather Kudyba[1,2], Mahnaz Minai[3], Motoshi Suzuki[4], Emanuela Tolosano[5], Derron A. Alvez[3], Jesus Valenzuela[1], Carolina Barillas-Mury[1], Shaden Kamhawi[1] and Joel Vega-Rodriguez[1,#]

[1] Laboratory of Malaria and Vector Research, National Institute of Allergy and Infectious Diseases, National Institutes of Health, Rockville, MD, 20852, USA

[2] Center for Drug Evaluation and Research, Food and Drug Administration, Silver Spring, MD, 20993, USA

[3] Infectious Disease Pathogenesis Section, National Institute of Allergy and Infectious Diseases, National Institutes of Health, Rockville, MD, 20852, USA

[4] Research Technologies Branch, National Institute of Allergy and Infectious Diseases, National Institutes of Health, 20852, Rockville, MD, USA.

[5] Molecular Biotechnology Center (MBC) "Guido Tarone", Department of Molecular Biotechnology and Health Sciences, University of Torino, 10126 Torino, Italy

Corresponding authors

Joel Vega-Rodriguez: joel.vega-rodriguez@nih.gov

Francis M. de Souza Saraiva: francis.desouzasaraiva@nih.gov

ABSTRACT

Blood feeding exposes arthropod vectors and the pathogens they transmit to toxic heme released during hemoglobin digestion. Although mammalian blood proteins can cross the mosquito midgut into the hemolymph, whether they remain biologically active within the vector is unknown. Proteomic analysis of *Anopheles gambiae* hemolymph identified mammalian proteins enriched by *Plasmodium* infection, including several involved in heme and iron metabolism. This enrichment was dependent on parasite invasion of the midgut epithelium. We show that mammalian hemopexin, a high-affinity heme scavenger, retains its heme-binding activity within mosquito tissues, where it mitigates heme toxicity, preserves midgut barrier integrity and microbiome homeostasis, and promotes *Plasmodium* development. These protective effects were lost with recombinant hemopexin unable to bind heme, establishing heme scavenging as the underlying mechanism. Hemopexin also promoted *Leishmania* parasite development in the sand fly and supported the fitness of *Aedes aegypti* and sand flies. Thus, parasite induced-redistribution of host hemopexin establishes a functional link between mammalian heme homeostasis, vector physiology, microbiome homeostasis and pathogen development, revealing a previously unrecognized host–vector–pathogen interaction and a potential vulnerability for transmission-blocking interventions.

INTRODUCTION

Blood ingestion presents significant physiological challenges for mosquitoes, other hematophagous vectors and the pathogens they transmit, particularly due to the vast amounts of heme released during hemoglobin digestion [1]. Heme (Fe-Protoporphyrin IX) is an iron-containing molecule that provides nutrients and signaling molecules essential for pathogen establishment and insect physiology, reproduction, and immune response [2, 3]. However, free labile heme is highly toxic since its iron induces the formation of reactive oxygen species (ROS) that initiate lipid peroxidation and membrane damage. Furthermore, the amphipathic nature of heme allows it to integrate into phospholipid membranes, altering membrane structure and inducing cell leakage [4-6]. To counteract

these threats, mosquitoes and parasites have evolved several mechanisms to manage heme toxicity. For example, *Plasmodium* parasites deploy antioxidant enzymes to counteract the oxidative stress encountered in the mosquito midgut and hemolymph [7-9]. In the case of mosquitoes, including *Anopheles*, protective mechanisms include the formation of a peritrophic matrix, a chitin- and glycoprotein-rich layer secreted by the midgut epithelium that separates the blood meal from epithelial cells. The peritrophic matrix facilitates the aggregation of heme into non-crystalline forms, reducing its capacity to induce ROS and membrane damage [10, 11]. Beyond the midgut lumen, mosquitoes utilize intracellular heme oxygenase to catalyze heme degradation and deploy antioxidant enzymes such as superoxide dismutase, catalase, and the thioredoxin and glutathione systems [12, 13]. Despite the effectiveness of these mechanisms, the sheer quantity of heme released during blood digestion raises the question of whether additional protective strategies exist, especially in scenarios where the midgut barrier is disrupted, such as during *Plasmodium* ookinete invasion, which allows heme to escape the peritrophic matrix barrier and interact directly with mosquito tissues.

Since 1980, a handful of studies have shown that specific proteins from the blood meal, such as immunoglobulins, albumin, and transferrin, can cross from the midgut lumen into the hemolymph of mosquitoes and other hematophagous arthropods [14-17]. However, whether mammalian proteins that enter an evolutionary distant blood-feeding arthropod retain their native biochemical functions and become functionally integrated into the vector physiology and pathogen development remains largely unexplored. Furthermore, whether pathogen infection itself can promote the redistribution of such host factors within the vector and thereby create conditions that favor its own development is unknown. In this study, we investigated whether mammalian blood proteins enriched in the mosquito hemolymph during *Plasmodium* infection remain biologically active and influence vector homeostasis, its associated microbiome, and parasite development. Proteomic analyses of hemolymph from *Anopheles gambiae* mosquitoes fed on *Plasmodium berghei*-infected mice identified mammalian proteins enriched following infection, including proteins associated with iron and heme metabolism. Focusing on hemopexin, a high-affinity heme scavenger highly enriched in

the hemolymph of infected mosquitoes, we found that it retains its native heme binding activity within the vector, buffers heme-associated oxidative stress, preserves midgut and microbiome homeostasis, and promotes *Plasmodium* development. These effects extend beyond the *Anopheles-Plasmodium* system, as host hemopexin also supports the fitness of other hematophagous dipterans and *Leishmania* development in sand flies. Together, our findings reveal a previously unrecognized host–vector–pathogen interaction in which *Plasmodium* invasion promotes the enrichment and redistribution of a mammalian protein within the vector, where it retains its native biochemical function and is exploited to support vector homeostasis and parasite transmission.

RESULTS

Blood proteins related to heme and iron metabolism are enriched in the hemolymph of infected mosquitoes

To determine whether blood proteins accumulate in the mosquito hemolymph, we performed label-free proteomic analysis of cell-free hemolymph from *An. gambiae* mosquitoes fed on uninfected or *P. berghei*-infected mice. Hemolymph was collected 30 h post-blood feeding to identify proteins crossing after the ookinete invades the midgut (Fig. 1A). Among the mouse-derived proteins detected in mosquito hemolymph, a subset defined by the presence of at least three unique peptides was enriched in infected mosquitoes (Fig. 1B-D and Supplementary Data 1). Although albumin was the most abundant mouse-derived proteins detected, hemoglobin subunits and hemopexin exhibited the highest fold enrichment in infected mosquitoes (Fig. 1D). Several of the enriched proteins, including hemoglobin, serotransferrin, albumin, and hemopexin, are associated with iron and heme metabolism.

Because blood digestion releases large amounts of heme [18], we focused on hemopexin, a high-affinity scavenger of labile heme, which was enriched 23-fold in infected mosquito hemolymph relative to uninfected controls (Fig. 1D and Supplementary Data 1). Western blot analyses of mosquito hemolymph detected hemopexin at an apparent molecular weight consistent with its native glycosylated form (65–70 kDa) and

the protein remained detectable in hemolymph up to 10 days after blood feeding (Fig 1E). When mosquitoes were infected with *P. berghei* deficient of the membrane attack ookinete protein (MAOP-KO), which form ookinetes that cannot invade the mosquito midgut [19], hemopexin levels in the hemolymph were indistinguishable from uninfected controls (Fig. 1F), indicating that hemopexin enrichment is dependent on ookinete midgut invasion.

Consistently, immunofluorescence analyses revealed increased hemopexin and hemoglobin staining in midguts from infected mosquitoes compared to uninfected controls (Fig. 1G-H, and Supplementary Figure 1A-B). In infected mosquitoes, both proteins were detected in invaded and non-invaded midgut cells, although invaded cells frequently displayed stronger staining. Hemopexin was also observed within epithelial cells in parasite-free regions of infected midguts (Fig. 1G, and Supplementary Figure 1A-B), indicating that its increased uptake is not restricted to sites of direct ookinete invasion or explained solely by local epithelial disruption. Although these experiments do not distinguish between permeability, active update, or a combination of mechanisms, they indicate that parasite invasion broadly promotes the redistribution of host proteins across the midgut epithelium. Finally, serum from *P. berghei*-infected mice collected before mosquito feeding exhibited elevated hemopexin levels relative to uninfected controls (Supplementary Fig. 2). Together, these findings indicate that *Plasmodium* infection promotes the accumulation of host hemopexin within the mosquito hemolymph during midgut invasion.

Hemopexin maintains physiological homeostasis in blood-fed mosquitoes

The enrichment of hemopexin in mosquito hemolymph following blood feeding suggested a functional role within the vector, leading us to examine its contribution to mosquito survival and reproductive fitness. To test this hypothesis, we utilized hemopexin-null (HPx-KO) mice [5, 6]. *An. gambiae* females fed on HPx-KO blood exhibited markedly reduced survival compared to mosquitoes fed on WT blood (Fig. 2A-B). Repeated blood feeding on HPx-KO mice reduced mosquito median survival from 35 to 15 days. A similar reduction in survival was observed after a single blood meal, with both infected and uninfected HPx-KO blood shortening mosquito lifespan relative to WT

controls (Supplementary Fig. 3A-B). In addition, mosquitoes fed on HPx-KO blood displayed reduced fecundity and fertility, as reflected by lower egg production and hatching rates (Fig. 2C-D).

To further investigate the systemic effects of hemopexin deficiency underlying these phenotypes, we performed transcriptomic analyses of midguts, carcasses, and ovaries from mosquitoes fed on WT or HPx-KO mice at 24 and 72 h post-blood feeding, together with sugar-fed controls. The most pronounced transcriptional differences were observed at 72 h post-feeding (Fig. 2E).

In the midgut, hemopexin deficiency triggered progressive transcriptional changes associated with oxidative stress and detoxification (Fig. 2E-F and Supplementary Data 2–3). At 24 h, genes involved in xenobiotic detoxification, including CYP6AK1, a UDP-glucuronosyltransferase, and ABCC11, were upregulated. By 72 h, cytochrome P450 genes (CYP6AG2, CYP6Z2, CYP6M2, and CYP6AK1) were strongly induced, whereas glutathione S-transferases (GSTD12, GSTE4, and GSTD6) and the ABC transporter ABCG18 were downregulated, a profile consistent with elevated oxidative stress. Genes associated with metabolism and nutrient uptake, including ILP5, TRYP6, ERD6-like, and glycogen debranching enzyme AGAP001200, were also altered, together with repression of ecdysone- and juvenile hormone-responsive genes (Eip74EF, Jhl-2137, Jhl-2008, and Jhl-3763), suggesting disruption of reproductive signaling pathways [20, 21].

Transcriptional alterations in carcasses and ovaries were limited at 24 h but became more pronounced at 72 h post-feeding (Fig. 2E, G-H and Supplementary Data 4–7). In carcasses, immune-related genes including cecropin-A, gambicin, and DPP4 were upregulated, consistent with activation of IMD/Rel2 signaling [22], whereas Toll/complement-associated genes, including defensin-2, CTLMA3, LRIM15, and the ficolins AGAP009184-RA and AGAP029325-RA, were downregulated [23]. Genes involved in lipid signaling and juvenile hormone metabolism, including PLD1/2, PLC, and the juvenile hormone esterase COEJHE2E, were also differentially expressed.

In ovaries, genes associated with juvenile hormone and ecdysone signaling, including juvenile hormone esterase (JHE), juvenile hormone-binding protein (JHBP), and the ecdysone-responsive gene E93, were differentially expressed, indicating disruption

of reproductive signaling pathways. In parallel, components of the insulin/mTOR pathway, including PI3K [24, 25], together with Marf/mitofusin (AGAP001802-RA), were induced, suggesting metabolic reprogramming and mitochondrial remodeling consistent with impaired reproductive homeostasis.

Together, these findings indicate that host hemopexin promotes mosquito survival and reproductive fitness while maintaining systemic physiological homeostasis during blood digestion.

Host hemopexin enhances vector competence by supporting *Plasmodium* development

Having established that hemopexin promotes mosquito physiological homeostasis, we next investigated how this host protein influences *Plasmodium* development across the mosquito life cycle. HPx-KO mice display elevated labile heme and altered systemic iron homeostasis during *Plasmodium* infection without changes in parasite burden or host mortality [6].

We first assessed the overall impact of hemopexin on mosquito infection by quantifying *P. berghei* oocysts at 7 dpi. *An. gambiae* mosquitoes fed on infected HPx-KO mice developed significantly fewer oocysts than mosquitoes fed on infected wild-type (WT) mice (Fig. 3A-B). Intravenous supplementation of HPx-KO mice with recombinant hemopexin restored infection to WT levels, whereas a heme-binding deficient mutant (HPx^{mut}) [26, 27] (Supplementary Fig. 4) failed to rescue parasite development, indicating that the protective effect of hemopexin depends on its heme-binding activity (Fig. 3B).

To define the stage at which hemopexin exerts this effect, we next examined early parasite development within the blood bolus. Midguts dissected at 2 dpi, after ookinete invasion and establishment of early oocysts, revealed significantly fewer parasites in mosquitoes fed on infected HPx-KO mice than in those fed on WT mice, whereas recombinant hemopexin supplementation restored parasite numbers (Fig.

3C). These findings indicate that hemopexin promotes parasite survival during the initial stages of mosquito infection.

Because hemopexin accumulates in mosquito hemolymph following infection, we then asked whether it also supports parasite development in the hemocoel after oocyst establishment. Mosquitoes were fed on *P. berghei*-infected HPx-KO mice and injected intrathoracically with recombinant hemopexin, heat-denatured hemopexin, or phosphate buffered saline (PBS) 48 h later, after oocyst formation (Fig. 3D). Recombinant hemopexin significantly increased oocyst numbers relative to control groups (Fig. 3E), indicating that hemopexin also promotes parasite development within the hemocoel.

Finally, we investigated whether the protective effect of hemopexin extends to human malaria parasites. *An. gambiae* mosquitoes were fed through membrane feeders containing *P. falciparum* gametocytes mixed with human erythrocytes and serum isolated from WT or HPx-KO mice (Fig. 3F). Similar to *P. berghei*, mosquitoes receiving HPx-KO serum developed significantly fewer *P. falciparum* oocysts, whereas recombinant hemopexin restored infection levels and HPx^{mut} failed to rescue parasite development (Fig. 3G).

Hemopexin limits oxidative damage and preserves midgut homeostasis during blood digestion

Successful blood digestion is essential for mosquito homeostasis and *Plasmodium* development within the vector, requiring coordinated homeostatic, digestive, and reproductive responses [20, 28, 29]. In this context, the peritrophic matrix contributes to midgut homeostasis by compartmentalizing the blood bolus and promoting heme detoxification [29, 30]. This prompted us to investigate the contribution of hemopexin to midgut barrier integrity. Transcriptomic analyses further suggested that mosquitoes fed on HPx-KO mice exhibit disrupted digestive and reproductive programs (Fig. 2E-F and Supplementary Data 2–3), supporting a broader disruption of midgut homeostasis.

Mosquitoes were fed on WT or HPx-KO blood supplemented with fluorescent dextran, and midguts dissected at 24 h post feeding were stained with wheat germ agglutinin (WGA) to visualize the peritrophic matrix. In mosquitoes fed on WT blood, dextran remained confined within the blood bolus, whereas mosquitoes fed on HPx-KO blood displayed extensive dextran diffusion into the epithelium together with severe disruption of the peritrophic matrix (Fig. 4A and Supplementary Fig. 5). To further assess midgut damage, transgenic *An. stephensi* mosquitoes expressing tdTomato in proliferating midgut stem cells were utilized [31]. Mosquitoes fed on HPx-KO blood exhibited increased tdTomato-positive cells, consistent with enhanced epithelial damage (Supplementary Fig. 6).

Disruption of the peritrophic matrix in HPx-KO-fed mosquitoes suggested that oxidative molecules derived from the blood bolus could damage midgut barriers and diffuse into mosquito tissues. Because hemopexin scavenges labile heme and limits heme-induced oxidative stress [32], systemic oxidative stress was evaluated in perfused hemolymph collected 24 h after blood feeding. Mosquitoes fed on HPx-KO blood exhibited significantly elevated hydrogen peroxide levels, lipid peroxidation markers (4HNE and MDA), and protein nitration relative to mosquitoes fed on WT blood (Fig. 4B-E). Supplementation of HPx-KO mice with recombinant hemopexin restored oxidative damage markers to WT levels, whereas the heme-binding deficient mutant HPx^{mut} failed to prevent oxidative damage (lipid peroxidation) (Fig. 4C-D), indicating that hemopexin protects mosquito tissues through its heme-binding activity.

Midgut microbiota contributes to peritrophic matrix formation, midgut homeostasis, and vector competence [29]. Therefore, the disruption of midgut barrier integrity and oxidative homeostasis observed in mosquitoes fed on HPx-KO mice suggested that microbiota dynamics could also be altered during blood digestion. Mosquitoes fed on HPx-KO blood exhibited a significant increase in bacterial load 24 h after feeding (Fig. 4F and Supplementary Fig. 7). Consistent with this observation, 16S sequencing revealed transient alterations in microbiota composition during early blood digestion. HPx-KO-fed mosquitoes exhibited increased alpha diversity at 48 h post-feeding, including higher observed ASVs and Shannon diversity, together with transient shifts in community structure that were no longer evident by 96 h

(Supplementary Fig. 8A, and C-D). Although PCoA based on Bray–Curtis dissimilarities did not reveal significant global differences in community composition, a trend toward separation was observed at 48 h post-feeding but not at 96 h (Supplementary Fig. 8B). Differential abundance analysis (DESeq2, FDR < 0.05) identified 31 genera associated with HPx-KO-fed mosquitoes at 48 h, including enrichment of Lactococcus, Curtobacterium, and Bryobacter (Fig. 4H and Supplementary Data 8 and 9). These findings indicate that hemopexin deficiency induces a transient disruption of microbiota homeostasis during early blood digestion.

Together, our data indicate that hemopexin protects mosquitoes from oxidative stress, preserves midgut barrier integrity, and maintains microbiota homeostasis during blood digestion.

The protective functions of hemopexin extend across blood-feeding vectors

The release of heme during blood digestion is a conserved feature of hematophagous insects. As a high-affinity heme scavenger, hemopexin could therefore provide similar protective functions across diverse blood-feeding vectors. To determine whether the effects of hemopexin extend beyond *Anopheles* mosquitoes, we investigated its role in *Aedes aegypti* and *Lutzomyia longipalpis*, together with the pathogens they transmit.

Similar to *An. gambiae*, *Ae. aegypti* mosquitoes fed on HPx-KO blood exhibited significantly reduced survival compared to mosquitoes fed on WT blood (Fig. 5A-B). Consistent with a conserved role in controlling heme-associated stress, hemolymph collected 48 h after blood feeding displayed elevated lipid peroxidation levels in HPx-KO-fed mosquitoes (Supplementary Fig. 9). To evaluate whether hemopexin also influences Dengue virus infection, mosquitoes were first maintained on WT or HPx-KO blood and subsequently infected using membrane feeders containing Dengue virus and erythrocytes isolated from HPx-KO mice, which are devoid of plasma and circulating hemopexin (Fig. 5C and Supplementary Fig. 10). Under these conditions, no differences in midgut viral loads were observed, indicating that hemopexin is not

required for the establishment of Dengue virus infection in the mosquito midgut (Fig. 5D and Supplementary Fig. 10).

We next assessed whether the effects of hemopexin extend to sand flies and *Leishmania* parasites. Similar to mosquitoes, *L. longipalpis* fed on HPx-KO blood exhibited reduced survival relative to flies fed on WT blood (Fig. 5E-F). Moreover, blood lacking hemopexin resulted in a significant reduction in both total *Leishmania donovani* parasite numbers and the proportion of infective metacyclic promastigotes within the sand fly midgut (Fig. 5G-H). Consistent with this effect, flies examined 21 days after blood feeding exhibited reduced parasite burdens, with a similar trend toward lower metacyclic differentiation in surviving insects (Supplementary Fig. 11).

Together, these findings uncover a conserved host-vector-pathogen interaction in which host hemopexin promotes physiological homeostasis in blood-feeding vectors while enhancing the development of diverse pathogens.

DISCUSSION

A growing body of evidence indicates that host blood proteins can traverse from the midgut lumen into the hemocoel of hematophagous arthropods, yet their functional significance remains unclear. Here, we show that *Plasmodium* infection promotes the enrichment and redistribution of mammalian hemopexin within the mosquito, where its activity is consistent with its heme-scavenging function and influences vector physiology, microbiome homeostasis, and parasite development. Supporting this conclusion, our proteomic analyses revealed that *Plasmodium* infection selectively enriches mammalian proteins involved in heme and iron metabolism within mosquito hemolymph. Among these, the high-affinity heme scavenger hemopexin [32] accumulated disproportionately relative to more abundant plasma proteins and in an ookinete invasion-dependent manner. Hemopexin was also detected within epithelial cells in regions without nearby parasites, suggesting that its uptake is not restricted to sites of direct parasite invasion or explained solely by local epithelial disruption. Whether this reflects increased permeability, selective transport, preferential retention, or a combination of mechanisms remains unclear. Regardless of the uptake mechanism, our findings show that hemopexin

becomes functionally integrated into the vector-microbiome-parasite system, buffered blood meal-derived heme and influencing oxidative homeostasis, midgut integrity, microbiota stability, reproduction, and *Plasmodium* parasite development in the mosquito.

The physiological importance of this host-derived factor is underscored by the broad fitness defects observed in insects fed on hemopexin-deficient blood. In addition to reduced survival, the absence of hemopexin impaired fertility and fecundity, indicating that disruption of midgut homeostasis has consequences that extend beyond the digestive tract. Transcriptomic analyses further suggest that hemopexin deficiency uncouples physiological processes normally coordinated during blood digestion and reproduction, resulting in widespread alterations in metabolic, reproductive, and stress-response pathways. Notably, OXR1, a regulator of oxidative stress responses in *Anopheles* [33], was induced only at 72 h post-feeding and, unlike during *P. berghei* infection, it was not accompanied by activation of canonical antioxidant effectors such as catalases and peroxidases. This pattern suggests that OXR1 contributes to adaptation to prolonged physiological stress rather than solely regulating antioxidant defenses. Because catalase-mediated detoxification of reactive oxygen species is a major determinant of mosquito fecundity [34], disruption of redox homeostasis may contribute directly to the reproductive defects observed in mosquitoes fed on hemopexin-deficient blood. Together, these findings identify mammalian hemopexin as an important determinant of vector fitness and reproductive success, key traits underlying vectorial capacity [35].

The importance of host-derived hemopexin is particularly striking given the extensive endogenous mechanisms hematophagous insects possess to manage heme toxicity, including sequestration within the peritrophic matrix, degradation by heme oxygenase, and multiple antioxidant pathways [1, 12]. Our findings therefore suggest that host-derived hemopexin is not merely an incidental component of the blood meal but an integral component of the heme-management strategy of blood-feeding insects. Because vertebrate hemopexin is consistently encountered during blood feeding, dipteran vectors and their pathogens may have evolved to exploit this host detoxification system as an additional layer of protection against heme-associated stress. Indeed, malaria parasite infection increased hemopexin levels in the blood. This role may extend beyond the

midgut, as hemopexin enters the mosquito hemolymph, where blood meal-derived iron is also present [36], providing a mechanism by which a mammalian heme-scavenging protein can influence the systemic environment encountered by the parasite during its development.

Because disruption of these barriers profoundly affects mosquito physiology and pathogen development [37-42], the broad phenotypes observed in mosquitoes fed on hemopexin-deficient blood are consistent with loss of compartmentalization normally imposed during blood digestion. The absence of major transcriptional changes in genes associated with peritrophic matrix formation further suggests that the defects observed in HPx-KO-fed mosquitoes arise from impaired matrix stability rather than defective synthesis. Increased exposure to labile heme likely contributes to this phenotype, as free heme promotes oxidative damage and can exacerbate hemolysis [43]. Notably, heme oxygenase was not induced despite evidence of increased heme-associated stress, consistent with previous studies showing that mosquito heme oxygenase is regulated primarily by nutrient-sensing pathways [12]. Together with the disruption of nutrient utilization and insulin/TOR-associated signaling in HPx-KO-fed mosquitoes, these findings suggest that hemopexin helps coordinate the physiological balance between blood digestion, heme metabolism, and reproductive investment. The increased accumulation of hemoglobin and hemopexin during ookinete invasion may therefore represent a compensatory response that helps preserve homeostasis in tissues exposed to blood-derived heme.

Consistent with its broader role in maintaining gut homeostasis, hemopexin deficiency was associated with transient dysbiosis during active blood digestion. Because these changes occurred in the absence of major regulation of midgut antimicrobial peptides, they likely reflect alterations in the digestive environment rather than local immune activation. Immune-related signatures nevertheless emerged in carcasses at later time points, consistent with previous studies showing that disruption of the peritrophic matrix promotes microbiota-dependent systemic immune responses [29]. The dysbiosis observed in HPx-KO-fed mosquitoes likely results from the combined effects of altered heme availability and oxidative stress. Although elevated ROS can restrict bacterial proliferation [44], increased exposure to heme and iron may favor taxa that

tolerate oxidative stress, leading to community restructuring rather than a uniform reduction in bacterial abundance. Such changes could further compromise barrier integrity and alter nutrient availability within the gut, potentially contributing to the disruption of insulin/TOR-associated signaling observed in HPx-KO-fed mosquitoes. In this context, hemopexin may function analogously to components of nutritional immunity by limiting access to iron from labile heme as a nutrient and helping maintain microbial homeostasis during blood digestion. Because the mosquito microbiota is an important determinant of *Plasmodium* development, these findings also identify the microbiome as another component of the host–vector–parasite interaction influenced by mammalian hemopexin. Whether the microbiome changes contribute directly to the parasite phenotype remains to be determined.

Beyond its effects on vector and microbiome homeostasis, hemopexin has a pronounced effect on parasite development. The absence of hemopexin in the blood meal significantly reduced *Plasmodium* infection, likely due to increased ROS-mediated parasite damage and potentially impaired iron acquisition, which is essential for *Plasmodium* development in the mosquito (Maya-Maldonado et al., 2021). Importantly, the protective effect of hemopexin on *Plasmodium* is not restricted to the blood bolus or the midgut environment. Direct injection of recombinant hemopexin into the hemolymph after oocyst formation restored parasite infection in mosquitoes fed on hemopexin-deficient blood, demonstrating that the mammalian protein can support *Plasmodium* oocysts development after the parasite has crossed the midgut. Together with the rescue of infection by recombinant hemopexin and the loss of protection with heme-binding-deficient hemopexin, these findings support heme sequestration as the biochemical mechanism linking hemopexin to both vector homeostasis and parasite survival. Thus, *Plasmodium* invasion promotes the enrichment and redistribution of a host-derived protective factor from which the parasite subsequently benefits during its development within the vector.

The effect on pathogens extends beyond *Plasmodium*. For *L. donovani* in sand flies, hemopexin deficiency impaired parasite survival and differentiation, sharing similarities with *Trypanosoma cruzi,* another trypanosomatid that relies on reduction of labile heme for successful differentiation within within its insect vector [45]. Interestingly,

Dengue virus infection in *Ae. aegypti* appeared unaffected by hemopexin deficiency under our experimental conditions, likely reflecting pathogen-specific differences in oxidative responses and antioxidant defenses [1, 44]. Thus, while the dependence on host hemopexin for physiological fitness was observed across the three dipteran vectors examined, its consequences for pathogen development appear to be context dependent. Nevertheless, the effects on two evolutionary distant eukaryotic parasites suggest that homeostasis of host-derived heme represents an important determinant of pathogen development within blood-feeding vectors.

Our findings reveal that *Plasmodium* invasion of the mosquito midgut promotes the redistribution of mammalian hemopexin within the vector, where its protective biochemical activity contributes to vector and microbiome homeostasis while creating conditions that favor parasite development. The extension of these effects to other blood-feeding dipterans and *Leishmania* parasites suggests a broader biological principle in which vectors and their pathogens exploit mammalian blood factors beyond their nutritional value. These results uncover a previously unrecognized host–vector–pathogen axis centered on heme homeostasis.

Materials and Methods

Mouse strains and ethical approval

All mouse procedures complied with NIH guidelines and were approved by the NIAID Animal Care and Use Committee under SOP LMVR 22. Wild-type C57BL/6 female mice (10–12 weeks old) were obtained from Charles River Laboratories, and hemopexin-null (HPx-KO; Hpx–/–) mice were provided by E. Tolosano and maintained in-house.

Anopheles rearing and *Plasmodium* infections

Anopheles gambiae (Keele) [46], *An. stephensi* (Nijmegen) [47], and the HP10 *An. stephensi* TdTomato^{+} line [31] were reared at 28 °C, 80% humidity, and a 12 h:12 h

photoperiod, with adults provided 10% sucrose. For *Plasmodium falciparum* NF54 infections, *An. stephensi* were membrane-fed with reconstituted human blood at 0.03% gametocytemia, prepared by mixing RBCs with human serum at 50% hematocrit; RBCs were reconstituted in heat-inactivated plasma from wild type (WT) or hemopexin-null (HPx-KO) mice, supplemented or not with 125 µg/mL recombinant hemopexin (rHPx) or mutant hemopexin (HPxmut), and oocysts were quantified 10 days post-infection after 0.2% mercurochrome staining. For *Plasmodium berghei* infections, *An. gambiae* were fed on WT or HPx-KO mice infected with a PbANKA mCherry–luciferase transgenic line [48] and maintained at 19 °C, 80% humidity, and a 12-h light–dark cycle; infection intensity was assessed by mCherry-fluorescent oocyst counts in dissected midguts at 2 days post-feeding (early oocysts) and 10 days post-feeding (late oocysts). For hemopexin reconstitution experiments, a group of mosquitoes (control) were allowed to feed on HPx-KO mice. The mice were then supplemented i.v. with 125 µg of rHPx or HPx^{mut} per mouse and 15 minutes later a second group of mosquitoes (experimental) were allowed to feed on the supplemented mouse.

For assays supplementing hemolymph with hemopexin, *An. gambiae* females were fed on *P. berghei*-infected HPx-KO mice. Mosquitoes were then injected intrathoracically with 100 ng hemopexin in PBS 48 h after infection, and *P. berghei oocyst* burdens were quantified as described above.

Cell-free hemolymph preparation

Cell-free hemolymph from uninfected or *P. berghei*–infected *An. gambiae* was collected from fully engorged females at 30 h and 10 days after blood feeding. The distal cuticle of the last abdominal segment was opened using fine forceps, and the hemocoel was flushed by gently injecting PBS supplemented with either protease inhibitor or 2 mg/mL 3-amino-1,2,4-triazole (AT) for hydrogen peroxide detection. The resulting hemolymph–PBS mixture was allowed to exit through the abdominal opening and collected using a pipette. Samples were immediately placed on ice and clarified by centrifugation at 3,500 × g for 5 min at 4 °C to remove circulating hemocytes and debris. The supernatant (cell-

free hemolymph) was transferred to fresh tubes and used immediately for downstream analyses or stored at –80 °C until use.

Proteomics of *Anopheles* cell-free hemolymph

For quantitative proteomics to compare hemolymph of *An. gambiae* which were fed on uninfected or *P. berghei*-infected mice, hemolymph samples collected at 30 h post-blood feeding were used. For each group, duplicated samples were investigated, where each sample was derived from hemolymph from 25 mosquitoes. These protein samples from cell-free mosquito hemolymph, approximately 50 µg-total, were separated by SDS–PAGE and visualized by Coomassie staining (ProtoBlue Safe, National Diagnostics). Gel lanes were excised, sectioned, and subjected to in-gel trypsin digestion. Briefly, gel pieces were destained in 50% acetonitrile/100 mM ammonium bicarbonate, reduced with dithiothreitol, alkylated with iodoacetamide, dehydrated in acetonitrile, and digested overnight at 30°C with sequencing-grade trypsin (Promega). Peptides were extracted in 50% acetonitrile with 5% formic acid, dried, then resuspended in water with 0.1% formic acid.

Peptides were analyzed by LC–MS/MS using an Orbitrap Fusion Lumos mass spectrometer coupled to an EASY-nLC 1200 system (Thermo Fisher Scientific). Samples were loaded onto a 2-cm PepMap C18 trap column and separated on a 2-cm PepMap C18 analytical column using a linear gradient of acetonitrile in 0.1% formic acid at a flow rate of 300 nL/min.

Data were acquired in data-dependent mode with MS1 scans in the Orbitrap (resolution 120,000) followed by MS2 fragmentation of multiply charged ions by collision-induced dissociation, scanning in the ion trap. Dynamic exclusion was set to 30 s.

Raw LC–MS/MS data were processed using MaxQuant (v2.0.3.0). Spectra were searched against a combined *Anopheles gambiae* and *Mus musculus* protein database, with common contaminants included. Enzyme specificity was set to trypsin, allowing up to two missed cleavages. Carbamidomethylation of cysteine was set as a fixed modification, and methionine oxidation and protein N-terminal acetylation were included as variable modifications. A false discovery rate (FDR) of 1% was applied at the peptide

and protein levels, and the match between runs feature was enabled. Protein quantification was performed using label-free quantification (LFQ) based on iBAQ intensities, and values were log2-transformed for downstream analyses. Only proteins identified with at least three unique peptides were retained, and contaminants were excluded. Downstream analyses were restricted to proteins assigned to the *Mus musculus* proteome.

Statistical analysis was performed in Perseus. LFQ intensities were median-centered, and missing values were imputed from a normal distribution. Differential abundance was assessed using Student's t-test with permutation-based FDR correction, with $q \leq 0.05$ considered significant.

Hemopexin detection by Western blot

Detection of hemopexin in hemolymph: Hemolymph from *An. gambiae* mosquitoes was collected 30 h and 10 days post–blood meal from uninfected and *P. berghei* infected mice. In separate experiments, mosquito hemolymph was collected 24 h after feeding on uninfected, *P. berghei*-infected, and MAOP-infected mice. Twenty micrograms of total protein from each pooled hemolymph or serum sample were mixed with SDS loading buffer and resolved on a 4–12% Bis-Tris SDS-PAGE gel (Bio-Rad). Proteins were transferred onto nitrocellulose membranes, blocked for 1 h in 5% bovine serum albumin (BSA) in PBST (PBS 1× + 0.1% Triton X-100), and incubated overnight at 4 °C with mouse Hemopexin Antibody (F-12) (Santa Cruz Biotechnology) at 1 µg/mL. After washing in PBST, membranes were incubated for 1 h at room temperature with an HRP-conjugated anti-mouse secondary antibody at a final concentration of 20 ng/mL. Signal was developed using SuperSignal™ West Femto Extended Duration Chemiluminescent Substrate (Thermo Fisher Scientific) and imaged on an iBright imaging system, and band intensities were quantified by densitometry in Adobe Photoshop. As loading controls, we used either a No-Stain™ Protein Labeling Reagent (Thermo Fisher Scientific), or a lipophorin antibody.

For detection of hemopexin in the mouse circulation, blood was obtained by cardiac puncture from uninfected or *P. berghei*-infected mice, and serum was separated by centrifugation at 3,500 × g for 15 minutes at 4 °C. SDS-PAGE and immunodetection were done as described above. Antibody against plasminogen was used as the loading control.

Ae. aegypti rearing and dengue virus infections

Ae. aegypti (Liverpool strain, LVP) were reared at 27 °C, 80% humidity, and a 12-h light–dark cycle, with adults maintained on 10% sucrose. Females 5–7 days old received two sequential blood meals on anesthetized WT or HPx-KO mice prior to dengue virus challenge. For the third feeding, dengue virus serotype 2 (DENV2; strain New Guinea C, GenBank AF038403, propagated in C6/36 cell line) was delivered by glass membrane feeding using RBCs (30% hematocrit) isolated from HPx-KO mice, supplemented or not with hemopexin (125 µg/mL), 1 mM ATP and virus-containing medium to a final titer of 5 × 10^6 PFU/mL. Mosquitoes were offered the infectious meal for 30 min at 37 °C, and fully engorged females were selected for downstream analyses. Five days post-feeding the midguts were dissected and placed in DMEM supplemented with 10% fetal bovine serum and 1% penicillin/streptomycin and kept at -70C until titration. For plaque assay, mosquito midgut homogenates were serially diluted in DMEM supplemented with 10% fetal bovine serum and 1% penicillin/streptomycin and each dilution was inoculated in a well of BHK-21 cell culture. The cells were incubated for 1h at 37°C and 5% CO_2 and then covered by a 0.8% methylcellulose in DMEM (2% FBS and 1% pen/strep) overlay. Five days later the medium was removed, the cells were incubated with 1% crystal violet in acetone:ethanol solution (1:1 v/v) for 1h and then washed out for plaque development.

Sand fly rearing and *Leishmania donovani* infections

Four- to six-day-old *Lutzomyia longipalpis* (Jacobina colony) female sand flies were reared at 26 °C, 75% humidity, and a 12-h light–dark cycle and maintained on 30% sucrose. For infections, rabbit defibrinated blood was spiked with 5 × 10^6 *Leishmania donovani* (MHOM/SD/62/1S) amastigotes per mL, isolated from a sick *L. donovani*–

infected hamster, and flies were allowed to feed for 2 h in the dark using an artificial membrane feeding system. Fully engorged females were separated and maintained under standard rearing conditions until transmission assays. Infection maturity was assessed 12 days post-infection, either after a single infected blood meal or after another uninfected blood meal was provided on day 6. The total parasite burden and the percentage of metacyclic promastigotes in individual dissected midguts (n = 5–10 flies) were quantified using a hemocytometer.

Insect fitness assays

An. gambiae

An. gambiae fitness was assessed in 5–7-day-old females that were blood-fed on anesthetized WT or HPx-KO mice. Survival was evaluated after either a single blood meal from infected or uninfected mice or a series of three blood meals from uninfected mice on days 0, 6, and 14, allowing completion of the gonotrophic cycle between feedings; mortality of 30 females per condition was monitored daily. For fecundity (eggs laid) and fertility (percent hatch), 20 fully engorged females were isolated individually after blood feeding. Oviposition was induced 72 h post-feeding with a small cup containing water lined with wet filter paper; eggs were counted at 24 and 48 h (the 48-hour total used as the fecundity response), and fertility was calculated as the percentage of eggs producing L1 larvae.

Ae. aegypti

Ae. aegypti fitness was assessed in 5–7-day-old females subjected to a three-blood-meal regimen on days 0, 8, and 15, with oviposition substrate provided between feedings to induce completion of the gonotrophic cycle. Mortality of 30 females per condition was monitored daily.

L. longipalpis

L. longipalpis fitness was assessed in 4–6-day-old females after either a single blood meal on day 0 or two blood meals on days 0 and 6 using anesthetized WT or HPx-KO

mice. Mortality of 300–500 females per condition was monitored daily for 21 days under standard insectary conditions.

Immunofluorescence assays

Midguts from fully engorged *An. gambiae* females 24 h post–blood meal on infected or uninfected mice were dissected in 1× PBS, opened longitudinally, washed to remove blood content, fixed in 4% paraformaldehyde, and washed three times. Tissues were blocked for 1 h in 5% BSA and 0.1% gelatin in PBST (PBS 1× + 0.1% Triton X-100), then incubated for 2 h with sheep anti-hemopexin or rabbit anti-hemoglobin antibodies at 2 µg/mL. After washing and an additional 1 h block, samples were incubated for 2 h with an Alexa Fluor 488–conjugated secondary antibody 1:1000. Midguts were washed and stained for 30 min with Alexa Fluor 647 Phalloidin at 165 nM and Hoechst 33342 at 2 µM in PBS, then mounted on Superfrost™ Plus slides using ProLong™ Gold Antifade Mountant. Imaging was performed on a Leica SP8 DMI 6000 confocal microscope using a 63× oil-immersion objective with sequential acquisition and variable z-stacks; images were processed in IMARIS 10.2, and final adjustments were made in Adobe Photoshop 27.1.

Hemolymph oxidative damage assays

Cell-free hemolymph from *An. gambiae* was collected from fully engorged females 24 h post–blood meal as described above. Hemolymph was flushed with PBS supplemented with protease inhibitor, and 10 µL was collected from each mosquito and pooled from 35 individuals per condition.

Lipid peroxidation was quantified by ELISA using rabbit anti–malondialdehyde (Abcam) and mouse anti–4-hydroxynonenal (clone 12F7) (Thermo Fisher) primary antibodies. Hemolymph was diluted to 20 µg/mL total protein, coated onto 96-well high-binding Maxisorp plates overnight at 4 °C, washed 10× with PBS-T (PBS 1× + 0.1% Triton X-100), blocked for 1 h in 5% BSA in PBS-T, incubated with primary antibodies at 2 µg/mL

for 2 h, washed again 10×, incubated for 1 h with species-specific HRP-conjugated secondary antibodies at 40 ng/mL, washed 10×, and developed with 1-Step™ Ultra TMB (Thermo Scientific) for 20 min before stopping with 0.1 N HCl and reading absorbance at 450 nm.

Nitrated proteins were detected from the same pooled hemolymph by Western blot using a mouse anti-nitrotyrosine antibody (Sigma-Aldrich). For H_2O_2 quantification, hemolymph was flushed with PBS containing 2 mg/mL 3-amino-1,2,4-triazole (AT), and 5 µL was collected from each mosquito and pooled from 10 individuals per condition; H_2O_2 levels were measured using the Amplex Red fluorimetric assay (Invitrogen) according to the manufacturer's instructions.

Quantification of tdTomato$^+$ midgut progenitor cells by confocal imaging

Midguts from *An. stephensi* HP10 [31] females were dissected 5 days after feeding on WT or HPx-KO mice. Dissections were made in 1× PBS, and midguts were opened longitudinally, and fixed in 4% paraformaldehyde for 30 min at room temperature. Tissues were washed three times in PBS, permeabilized for 30 min in PBST (PBS 1× + 0.1% Triton X-100), counterstained for 30 min with Hoechst 33342 (20 µM), washed, and mounted luminal side up on Superfrost™ Plus slides using ProLong™ Gold Antifade Mountant. tdTomato$^+$ cells were imaged on a Leica SP8 DMI 6000 confocal microscope using a 63× oil-immersion objective with sequential acquisition and z-stacks spanning the epithelial layer. tdTomato$^+$ cell volumes and nuclear-normalized measurements were quantified in IMARIS 10.2 following the methodology described in [31]. Final image adjustments were performed in Adobe Photoshop 27.1.

Peritrophic matrix integrity microscopy

An. gambiae females were fed blood supplemented with Alexa Fluor 488 dextran (10 kDa) dextran from WT or HPx-KO mice, and midguts were collected 24 h post–blood meal. Dissected midguts were fixed in 10% neutral buffered formalin, processed using a Leica

ASP6025 tissue processor, embedded in paraffin, and sectioned at 5 μm. Sections were deparaffinized and rehydrated through graded ethanol and xylene washes, then stained for 2 h with Alexa Fluor 647 conjugated Wheat Germ Agglutinin (WGA) at 0.5 μg/mL to label the peritrophic matrix. After PBS washes and clearing in graded alcohol and xylene, sections were mounted with permanent mounting medium and coverslipped. Dextran fluorescence was imaged directly from the sections on a Leica SP8 DMI 6000 confocal microscope using a 63× oil-immersion objective with sequential acquisition of dextran and WGA channels. Peritrophic matrix integrity was evaluated by determining whether dextran remained confined within the blood bolus or showed leakage beyond the peritrophic matrix boundary.

qPCR analysis of midgut bacterial load and gene expression

Total RNA was extracted from individual midguts using TRIzol reagent (Thermo Fisher Scientific) according to the manufacturer's instructions. RNA samples were treated with gDNA Wipeout for 5 min at 42 °C, and cDNA was synthesized using the QuantiTect Reverse Transcription Kit (Qiagen) for 30 min. Quantitative PCR (qPCR) was performed using the DyNamo SYBR Green qPCR Kit (Thermo Fisher Scientific) on a CFX96 Real-Time PCR Detection System (Bio-Rad). The S7 ribosomal protein gene was used as the endogenous control for mosquito gene-expression analyses [49]. Total bacterial load was quantified using 16S rRNA primers as described in [42]. Relative expression and abundance values were calculated using the ΔCt method [50].

Metagenomic analysis of mosquito midgut samples

Midgut microbiota composition was assessed by 16S rRNA gene amplicon sequencing. Midguts from *An. gambiae* females were dissected individually in single droplets of sterile 1× PBS, and pools of 15 midguts per condition were generated for samples collected at 48- or 96-h post–blood meal. Pooled midgut samples were immediately frozen, and DNA extraction, library preparation, and sequencing were performed by Novogene using their validated bacterial 16S rRNA V4 primer set and a high-throughput Illumina platform.

Bioinformatic processing, including quality filtering, denoising, and taxonomic assignment, was carried out with the provider's in-house analysis pipeline. Microbial community structure was evaluated through alpha- and beta-diversity analyses, including Shannon and Simpson diversity indices, and ordination-based comparisons of community composition.

Microbial community structure was assessed using alpha- and beta-diversity metrics. Alpha diversity was quantified using observed richness (Observed ASVs) and the Shannon diversity index, and differences between HPxKO and control mosquitoes were evaluated using pairwise comparison within each timepoint (48h and 96h post blood meal). Beta diversity was assessed in MicrobiomeAnalyst using Bray-Curtis dissimilarities and visualized by Principal coordinates analysis (PCoA). Differences in community composition were tested using permutational multivariate analysis of variance (PERMANOVA) based on the experimental grouping factor (Ctrl-48h, Ctrl-96h, HPxKO-48h and HPxKO-96h). A global PERMANOVA was performed across all four groups, followed by pairwise PERMANOVA comparisons among groups with Benjamini-Hochberg false discovery rate (FDR) correction. The homogeneity of multivariate dispersion was evaluated using PERMDISP to test group separation and dispersion.

To identify genera associated with HPxKO, we performed differential abundance analyses using DESeq2. Comparisons were conducted separately at 48h and 96h post-blood meal using a single-factor design (HPxKO vs control). DESeq2 was used with its default normalization, and results are reported as log2 fold changes (log2FC). Multiple testing correction was performed using the Benjamini-Hochberg false discovery rate (FDR). Volcano plots were generated for each time point to graph differential abundance results, with genera meeting the significance level (FDR<0.05) and the pre-defined effect-size threshold highlighted in orange. Hierarchical clustered heatmaps were generated in R using genus-level normalized abundance tables after total sum scaling (TSS) to provide a genus-level comparison of abundance patterns and clustering at each time point for the top 20 genera. Genera abundances were autoscaled (z-score per genus), and hierarchical clustering was performed using Euclidean distance with Ward linkage. All plots were generated in R using ggplot2 and ggrepel packages.

We analyzed 48h and 96h separately because they represent distinct post-blood meal stages and mosquito gut communities can shift rapidly over this period. Pooling of these two time points would confound HPxKO effects with the natural progression of the gut community after feeding, which would make the results difficult to interpret. In this manner, we graphed composition and ordination using all the samples to provide an overall overview but ran statistical tests (alpha diversity and DESeq2 differential abundance) separately at each time point by comparing HPxKO and control mosquitoes at 48h and at 96h to assess whether dysbiosis was detectable at each time point.

Transcriptome sequencing and differential expression analysis

Mosquitoes were fed on either wild-type (WT) or hemopexin-deficient (HPx-KO) mice, and tissues were collected for transcriptome analysis. Total RNA was isolated from mosquito midguts using TRIzol reagent, while carcass and ovary samples were preserved in RNAlater prior to extraction. RNA integrity and concentration were assessed using the Agilent 2100 Bioanalyzer and NanoDrop spectrophotometer, and only high-quality samples were used for library preparation. Strand-specific RNA-seq libraries were generated and sequenced on an Illumina platform to produce paired-end reads. Adapter sequences and low-quality reads were removed to obtain clean reads for downstream analyses.

Clean reads were mapped to the *Anopheles gambiae* reference genome using a splice-aware aligner, and gene expression levels were quantified for each sample. Differential expression analysis was performed between mosquitoes fed on WT and HPx-KO mice, stratified by tissue (midgut, carcass, and ovaries) and time point (24 h and 72 h). Genes with a false discovery rate (FDR) < 0.05 and an absolute log2 fold change ≥ 1 were considered differentially expressed. Functional enrichment analysis of differentially expressed genes was conducted using Gene Ontology (GO) and KEGG pathway annotations.

Data availability

All data needed to evaluate the conclusions are included in the manuscript and or the supplementary materials.

REFERENCES

1. Sterkel, M., et al., *The Dose Makes the Poison: Nutritional Overload Determines the Life Traits of Blood-Feeding Arthropods.* Trends Parasitol, 2017. **33**(8): p. 633-644.
2. Harizanova, N., et al., *Aedes aegypti transferrin. Gene structure, expression pattern, and regulation.* Insect Mol Biol, 2005. **14**(1): p. 79-88.
3. Cardoso-Jaime, V., N.A. Broderick, and K. Maya-Maldonado, *Metal ions in insect reproduction: a crosstalk between reproductive physiology and immunity.* Curr Opin Insect Sci, 2022. **52**: p. 100924.
4. Schmitt, T.H., W.A. Frezzatti, Jr., and S. Schreier, *Hemin-induced lipid membrane disorder and increased permeability: a molecular model for the mechanism of cell lysis.* Arch Biochem Biophys, 1993. **307**(1): p. 96-103.
5. Tolosano, E., et al., *Defective recovery and severe renal damage after acute hemolysis in hemopexin-deficient mice.* Blood, 1999. **94**(11): p. 3906-14.
6. Ramos, S., et al., *Targeting circulating labile heme as a defense strategy against malaria.* Life Sci Alliance, 2024. **7**(4).
7. Vega-Rodriguez, J., et al., *The glutathione biosynthetic pathway of Plasmodium is essential for mosquito transmission.* PLoS Pathog, 2009. **5**(2): p. e1000302.
8. Pastrana-Mena, R., et al., *Glutathione reductase-null malaria parasites have normal blood stage growth but arrest during development in the mosquito.* J Biol Chem, 2010. **285**(35): p. 27045-27056.
9. Turturice, B.A., et al., *Expression of cytosolic peroxiredoxins in Plasmodium berghei ookinetes is regulated by environmental factors in the mosquito bloodmeal.* PLoS Pathog, 2013. **9**(1): p. e1003136.
10. Pascoa, V., et al., *Aedes aegypti peritrophic matrix and its interaction with heme during blood digestion.* Insect Biochem Mol Biol, 2002. **32**(5): p. 517-23.
11. Devenport, M., et al., *Identification of the Aedes aegypti peritrophic matrix protein AeIMUCI as a heme-binding protein.* Biochemistry, 2006. **45**(31): p. 9540-9.
12. Bottino-Rojas, V., et al., *Non-canonical transcriptional regulation of heme oxygenase in Aedes aegypti.* Sci Rep, 2019. **9**(1): p. 13726.
13. Pereira, L.O., et al., *Biglutaminyl-biliverdin IX alpha as a heme degradation product in the dengue fever insect-vector Aedes aegypti.* Biochemistry, 2007. **46**(23): p. 6822-9.
14. Vaughan, J.A. and A.F. Azad, *Passage of host immunoglobulin G from blood meal into hemolymph of selected mosquito species (Diptera: Culicidae).* J Med Entomol, 1988. **25**(6): p. 472-4.
15. Nogge, G. and M. Giannetti, *Specific antibodies: a potential insecticide.* Science, 1980. **209**(4460): p. 1028-9.
16. Mori, H., et al., *Host-derived transferrin is maintained and transferred from midgut to ovary in Haemaphysalis longicornis ticks.* Ticks Tick Borne Dis, 2014. **5**(2): p. 121-6.
17. Meyers, J.I., M. Gray, and B.D. Foy, *Mosquitocidal properties of IgG targeting the glutamate-gated chloride channel in three mosquito disease vectors (Diptera: Culicidae).* J Exp Biol, 2015. **218**(Pt 10): p. 1487-95.
18. Peterson, T.M., A.J. Gow, and S. Luckhart, *Nitric oxide metabolites induced in Anopheles stephensi control malaria parasite infection.* Free Radic Biol Med, 2007. **42**(1): p. 132-42.

19. Kadota, K., et al., *Essential role of membrane-attack protein in malarial transmission to mosquito host.* Proc Natl Acad Sci U S A, 2004. **101**(46): p. 16310-5.
20. Noriega, F.G., *Nutritional regulation of JH synthesis: a mechanism to control reproductive maturation in mosquitoes?* Insect Biochem Mol Biol, 2004. **34**(7): p. 687-93.
21. Ekoka, E., et al., *20-Hydroxyecdysone (20E) signaling as a promising target for the chemical control of malaria vectors.* Parasit Vectors, 2021. **14**(1): p. 86.
22. Zakovic, S. and E.A. Levashina, *NF-kappaB-Like Signaling Pathway REL2 in Immune Defenses of the Malaria Vector Anopheles gambiae.* Front Cell Infect Microbiol, 2017. **7**: p. 258.
23. Meister, S., et al., *Immune signaling pathways regulating bacterial and malaria parasite infection of the mosquito Anopheles gambiae.* Proc Natl Acad Sci U S A, 2005. **102**(32): p. 11420-5.
24. Huang, J. and B.D. Manning, *A complex interplay between Akt, TSC2 and the two mTOR complexes.* Biochem Soc Trans, 2009. **37**(Pt 1): p. 217-22.
25. Zhao, W., et al., *Juvenile hormone induces phosphorylation of insulin/insulin-like growth factor signaling proteins in previtellogenic Aedes aegypti mosquitoes.* Insect Sci, 2024.
26. Morgan, W.T., et al., *Identification of the histidine residues of hemopexin that coordinate with heme-iron and of a receptor-binding region.* J Biol Chem, 1993. **268**(9): p. 6256-62.
27. Smith, A. and W.T. Morgan, *Hemopexin-mediated heme uptake by liver. Characterization of the interaction of heme-hemopexin with isolated rabbit liver plasma membranes.* J Biol Chem, 1984. **259**(19): p. 12049-53.
28. Hansen, I.A., et al., *Four-way regulation of mosquito yolk protein precursor genes by juvenile hormone-, ecdysone-, nutrient-, and insulin-like peptide signaling pathways.* Front Physiol, 2014. **5**: p. 103.
29. Rodgers, F.H., et al., *Microbiota-induced peritrophic matrix regulates midgut homeostasis and prevents systemic infection of malaria vector mosquitoes.* PLoS Pathog, 2017. **13**(5): p. e1006391.
30. Magalhaes, T., *What is the association of heme aggregates with the peritrophic matrix of adult female mosquitoes?* Parasit Vectors, 2014. **7**: p. 362.
31. Barletta, A.F., et al., *Mosquito midgut stem cell cellular defense response limits Plasmodium parasite infection.* Nat Commun, 2024. **15**(1): p. 1422.
32. Li, Y., et al., *Double-edged functions of hemopexin in hematological related diseases: from basic mechanisms to clinical application.* Front Immunol, 2023. **14**: p. 1274333.
33. Jaramillo-Gutierrez, G., et al., *The Anopheles gambiae oxidation resistance 1 (OXR1) gene regulates expression of enzymes that detoxify reactive oxygen species.* PLoS One, 2010. **5**(6): p. e11168.
34. DeJong, R.J., et al., *Reactive oxygen species detoxification by catalase is a major determinant of fecundity in the mosquito Anopheles gambiae.* Proc Natl Acad Sci U S A, 2007. **104**(7): p. 2121-6.
35. Smith, D.L. and F.E. McKenzie, *Statics and dynamics of malaria infection in Anopheles mosquitoes.* Malar J, 2004. **3**: p. 13.
36. Zhou, G., et al., *Fate of blood meal iron in mosquitoes.* J Insect Physiol, 2007. **53**(11): p. 1169-78.
37. Baia-da-Silva, D.C., et al., *The role of the peritrophic matrix and red blood cell concentration in Plasmodium vivax infection of Anopheles aquasalis.* Parasit Vectors, 2018. **11**(1): p. 148.
38. Coutinho-Abreu, I.V., et al., *Targeting the midgut secreted PpChit1 reduces Leishmania major development in its natural vector, the sand fly Phlebotomus papatasi.* PLoS Negl Trop Dis, 2010. **4**(11): p. e901.
39. Niu, G., et al., *The fibrinogen-like domain of FREP1 protein is a broad-spectrum malaria transmission-blocking vaccine antigen.* J Biol Chem, 2017. **292**(28): p. 11960-11969.
40. Pimenta, P.F., et al., *A novel role for the peritrophic matrix in protecting Leishmania from the hydrolytic activities of the sand fly midgut.* Parasitology, 1997. **115 (Pt 4)**: p. 359-69.

41. Pruzinova, K., et al., *Leishmania mortality in sand fly blood meal is not species-specific and does not result from direct effect of proteinases.* Parasit Vectors, 2018. **11**(1): p. 37.
42. Talyuli, O.A.C., et al., *The Aedes aegypti peritrophic matrix controls arbovirus vector competence through HPx1, a heme-induced peroxidase.* PLoS Pathog, 2023. **19**(2): p. e1011149.
43. Balla, J., et al., *Heme, heme oxygenase and ferritin in vascular endothelial cell injury.* Mol Nutr Food Res, 2005. **49**(11): p. 1030-43.
44. Oliveira, J.H., et al., *Blood meal-derived heme decreases ROS levels in the midgut of Aedes aegypti and allows proliferation of intestinal microbiota.* PLoS Pathog, 2011. **7**(3): p. e1001320.
45. Nogueira, N.P., et al., *Proliferation and differentiation of Trypanosoma cruzi inside its vector have a new trigger: redox status.* PLoS One, 2015. **10**(2): p. e0116712.
46. Hurd, H., et al., *Evaluating the costs of mosquito resistance to malaria parasites.* Evolution, 2005. **59**(12): p. 2560-72.
47. Feldmann, A.M. and T. Ponnudurai, *Selection of Anopheles stephensi for refractoriness and susceptibility to Plasmodium falciparum.* Med Vet Entomol, 1989. **3**(1): p. 41-52.
48. Prado, M., et al., *Long-term live imaging reveals cytosolic immune responses of host hepatocytes against Plasmodium infection and parasite escape mechanisms.* Autophagy, 2015. **11**(9): p. 1561-79.
49. Molina-Cruz, A., et al., *Reactive oxygen species modulate Anopheles gambiae immunity against bacteria and Plasmodium.* J Biol Chem, 2008. **283**(6): p. 3217-3223.
50. Pfaffl, M.W., *A new mathematical model for relative quantification in real-time RT-PCR.* Nucleic Acids Res, 2001. **29**(9): p. e45.

Acknowledgements

This research was supported [in part] by the Intramural Research Program of the National Institutes of Health (NIH). The contributions of the NIH author(s) are considered Works of the United States Government. The findings and conclusions presented in this paper are those of the author(s) and do not necessarily reflect the views of the NIH or the U.S. Department of Health and Human Services.

The authors are grateful to, Andre Laughinghouse, Kevin Lee and Claudio Meneses for insectary support; Allison Rooth and DeAndre Bacon for technical support with animals. Ming Zhao for technical support with proteomics sample processing. This work was funded by NIH Distinguished Scholars Program and the Intramural Research Program of the Division of Intramural Research (AI001250-01), National Institute of Allergy and Infectious Diseases, NIH to J.V.R.

Author Contributions

F.M.d.S.S., T.L.A.-S., and J.V.-R. conceived and designed the study. F.M.d.S.S., T.L.A.-S., O.A.C.T., E.I., A.B.B.F., R.E.J, R.C. and S.K. performed experiments and data analysis. P.H.A., M.M., D.A., and M.S performed assays and provided technical expertise essential for the research. E.T. provided key resources and technical expertise essential for the research. J.V.-R. supervised the project. F.M.d.S.S. drafted the manuscript, and all authors contributed to manuscript revision and approved the final version.

Competing Interests

The authors declare no competing interest. All data are available in the manuscript or the supplementary materials.

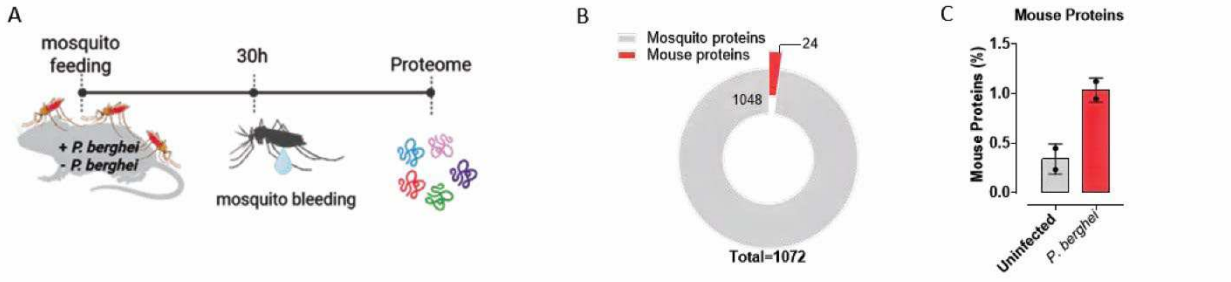

D

Protein IDs	FC	Unique peptides	Unique sequence coverage [%]	Mol. weight [kDa]
Hemoglobin subunit beta-2	30.642	6	46.3	15.878
Hemopexin	23.015	13	36.7	51.317
Hemoglobin subunit alpha	6.220	5	56.3	15.112
Alpha-1-antitrypsin	3.622	5	14.3	45.854
Serotransferrin	3.279	36	56.4	76.723
Albumin	2.075	36	71.7	68.692
Desmoplakin	0.977	15	8	332.91
Carboxylesterase 1	0.841	5	13.5	61.055
Glyceraldehyde-3-phosphate dehydrogenase	0.776	4	19.5	31.521
Annexin A2	0.763	8	27.7	38.676
Junction plakoglobin	0.716	7	13.2	81.8
Carbonic anhydrase 2	*	6	40	29.032

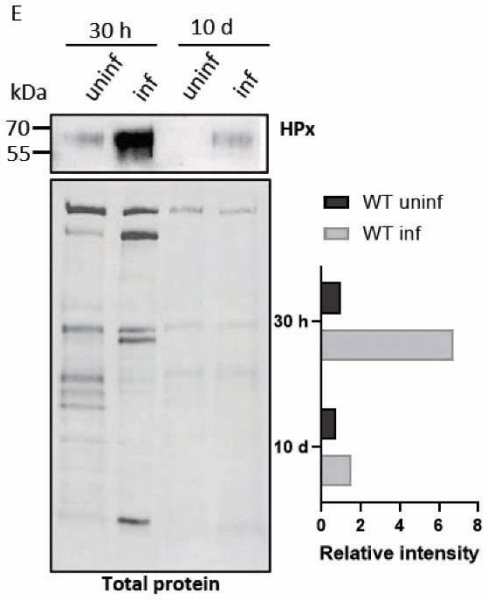

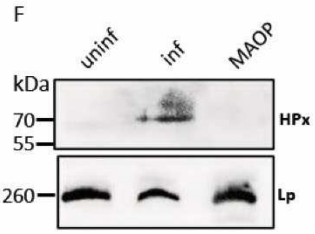

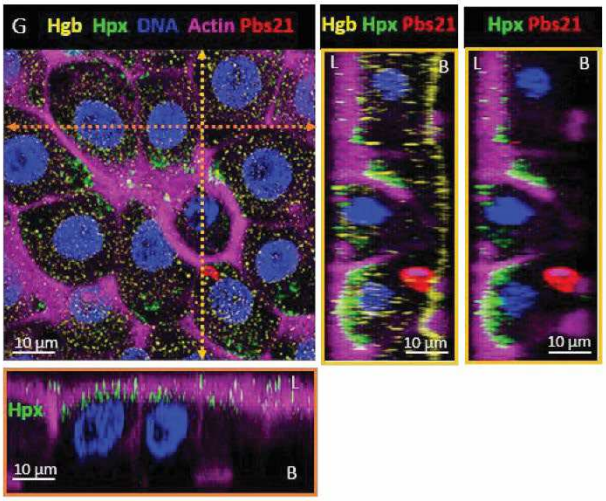

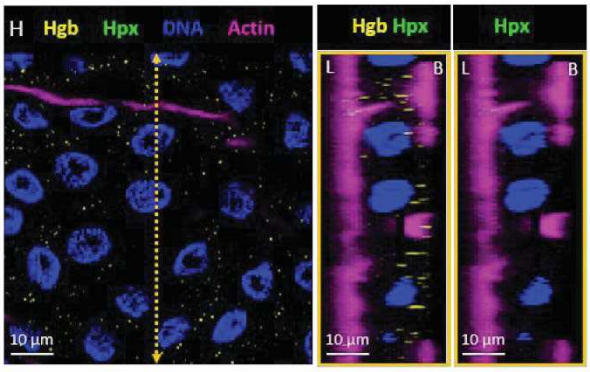

877

Figure 1. Plasmodium midgut invasion promotes the enrichment in the mosquito hemolymph of mammalian proteins associated with heme metabolism. (A) Experimental design. *An. gambiae* mosquitoes were fed on either uninfected or *P. berghei*-infected mice. Cell-free hemolymph was collected by perfusion at 30 h post-blood feeding and analyzed by label-free proteomics. (B) Protein source distribution in the mosquito hemolymph proteome. The donut chart shows the number of mosquito- and mouse-derived proteins identified by proteomic analysis. Numbers indicate the total proteins identified from each source. (C) Percentage of mouse-derived proteins detected in the hemolymph proteome of mosquitoes fed on uninfected or *P. berghei*-infected mice. Bars represent mean ± SEM. (D) Mouse-derived proteins identified in mosquito hemolymph. Proteins detected with at least three unique peptides are shown. FC: fold change in infected versus uninfected. Asterisks indicate proteins detected exclusively in infected samples. (E) Detection of hemopexin (HPx) in mosquito hemolymph by Western blot. Uninf: uninfected, inf: *P. berghei*-infected. Representatives immunoblot (top) and total protein staining used as a loading control (bottom). Relative HPx signal intensities are shown on the right. (F) HPx detection in the hemolymph of mosquitoes fed on uninfected mice (uninf), mice infected with wild-type *P. berghei* (inf), or mice infected with MAOP-knockout (*MAOP*-KO) *P. berghei*. Lp: lipophorin. Representative data from three independent experiments. (G–H) Localization of hemoglobin (Hgb) and hemopexin (HPx) in mosquito midguts by immunofluorescence microscopy. (G) Midguts from mosquitoes fed on *P. berghei*-infected mice. Ookinetes were detected with an anti-Pbs21 antibody (red), HPx is shown in green, Hgb in yellow, actin in magenta, and nuclei (DNA) in blue. Orthogonal views corresponding to the indicated xy planes are shown. (H) Midguts from mosquitoes fed on uninfected mice stained for Hgb (yellow), HPx (green), actin (magenta), and DNA (blue). L, lumen; B, basal side.

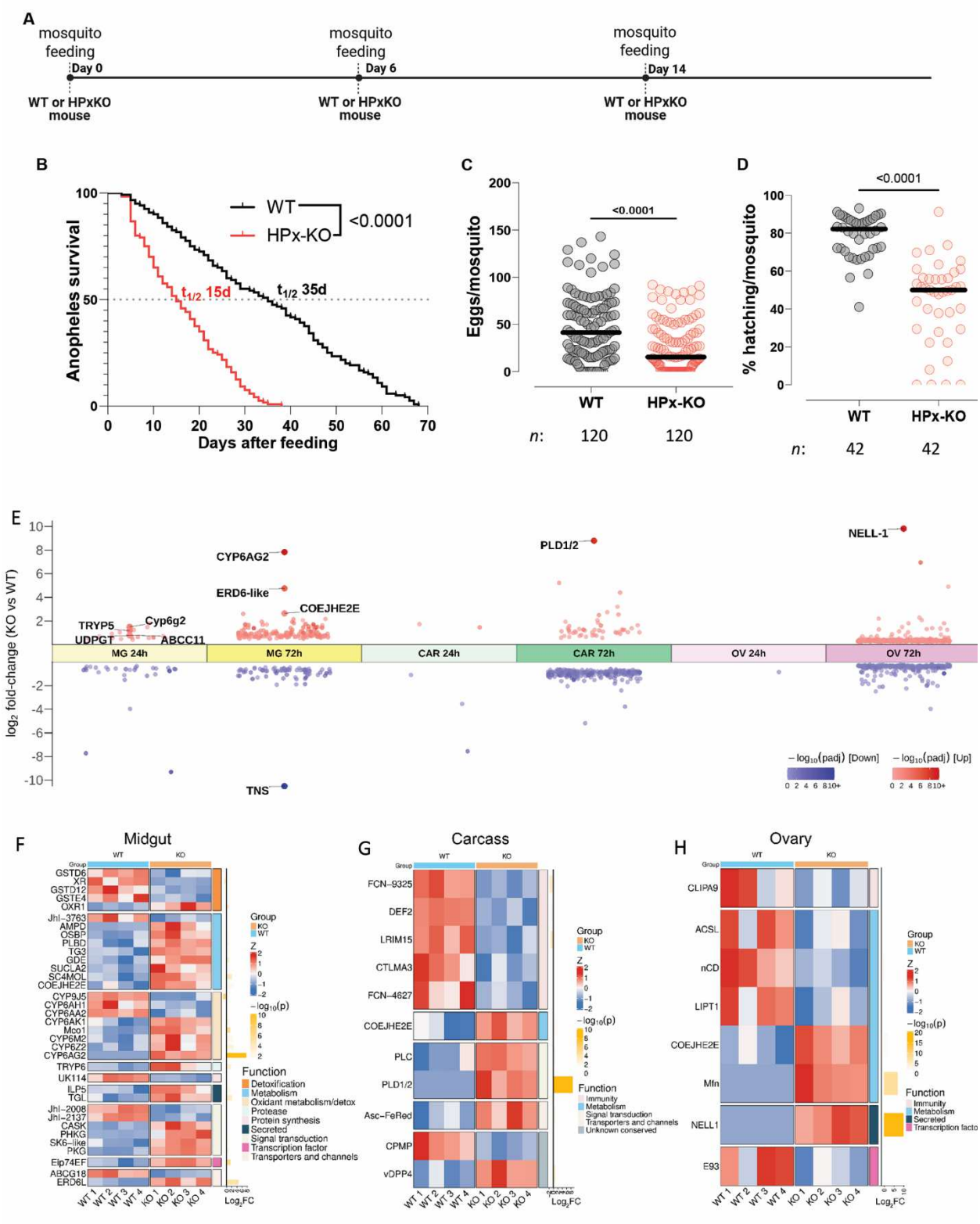

907

908 **Figure 2. Host hemopexin supports mosquito physiological homeostasis and**
909 **fitness.** (A) Experimental design. *An. gambiae* mosquitoes were fed on uninfected wild-

type (WT) or hemopexin-deficient (HPx-KO) mice on days 0, 6, and 14. (B) Kaplan–Meier survival curves of mosquitoes fed on WT or HPx-KO mice. Dotted line indicates 50% survival ($t_{1/2}$). Statistical significance was assessed using the log-rank (Mantel–Cox) test. (C-D) Number of eggs laid per mosquito (C) and hatching rate (D) following blood feeding on WT or HPx-KO mice. Each dot represents an individual mosquito (C) or individual egg hatching (D). Horizontal lines indicate median values. Statistical significance was determined using the Mann–Whitney test. (E) Distribution of differentially expressed genes (DEGs) in mosquitoes fed on HPx-KO mice relative to WT controls. Each point represents a DEG in the midgut (MG), carcass (CAR), or ovary (OV) at 24 h or 72 h after blood feeding. The y-axis shows $\log_2$ fold change (KO vs WT), and point color intensity reflects the adjusted p-value (padj). Selected genes are indicated. (F–H) Heatmaps showing expression profiles of DEGs at 72 h after blood feeding in the midgut (F), carcass (G), and ovary (H) of mosquitoes fed on WT or HPx-KO mice. Rows correspond to genes grouped according to predicted functional categories, and columns represent biological replicates. Color intensity indicates standardized expression values (Z-scores). Functional classifications and corresponding $-\log_{10}(p)$ values are shown alongside each heatmap. Data from two independent feeding experiments performed in duplicate (n = 15 mosquitoes per condition).

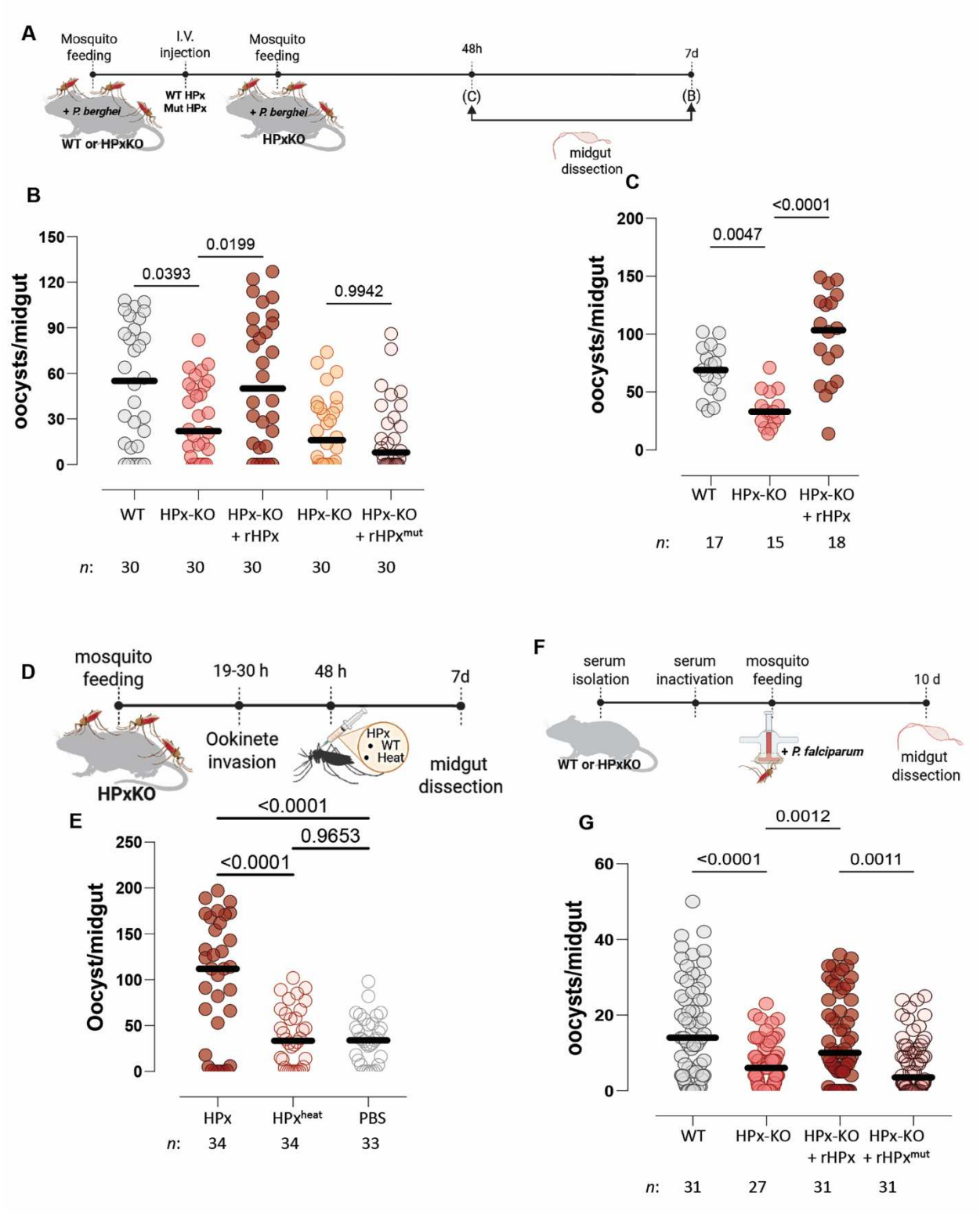

Figure 3. Hemopexin promotes *Plasmodium* infection through its heme-binding activity and supports oocyst survival after midgut invasion. (A-C) Experimental

design (A). *An. gambiae* mosquitoes were fed on *P. berghei*-infected wild-type (WT) or hemopexin-deficient (HPx-KO) mice. HPx-KO mice received intravenous injections of recombinant hemopexin (rHPx) or a heme-binding-deficient mutant form ($rHPx^{mut}$) before mosquito feeding. Early (B) and late (C) oocyst development were assessed by midgut dissections at 48 h and 7 days post-feeding, respectively. (D-E) Experimental design to assess the effect of hemolymph HPx on oocyst survival after midgut invasion (D). Mosquitoes fed on *P. berghei*-infected HPx-KO mice received intrathoracic injections of native HPx, heat-inactivated HPx (HPx^{heat}), or PBS at 48 h post-feeding, after oocyst formation. Oocyst numbers were determined 7 days after infection (E). (F-G) Experimental design for *P. falciparum* infections (F). Serum was collected from WT or HPx-KO mice, heat-inactivated, and used in standard membrane feeding assays supplemented with *P. falciparum* gametocyte cultures. Midguts were dissected 10 days after infection for oocyst quantification (G). Representative experiments selected from three independent assays (B, C, and G) or two independent assays (E) are shown. Each dot represents one mosquito midgut, and horizontal bars indicate median values. Statistical significance was evaluated by one-way ANOVA followed by Tukey's post hoc test.

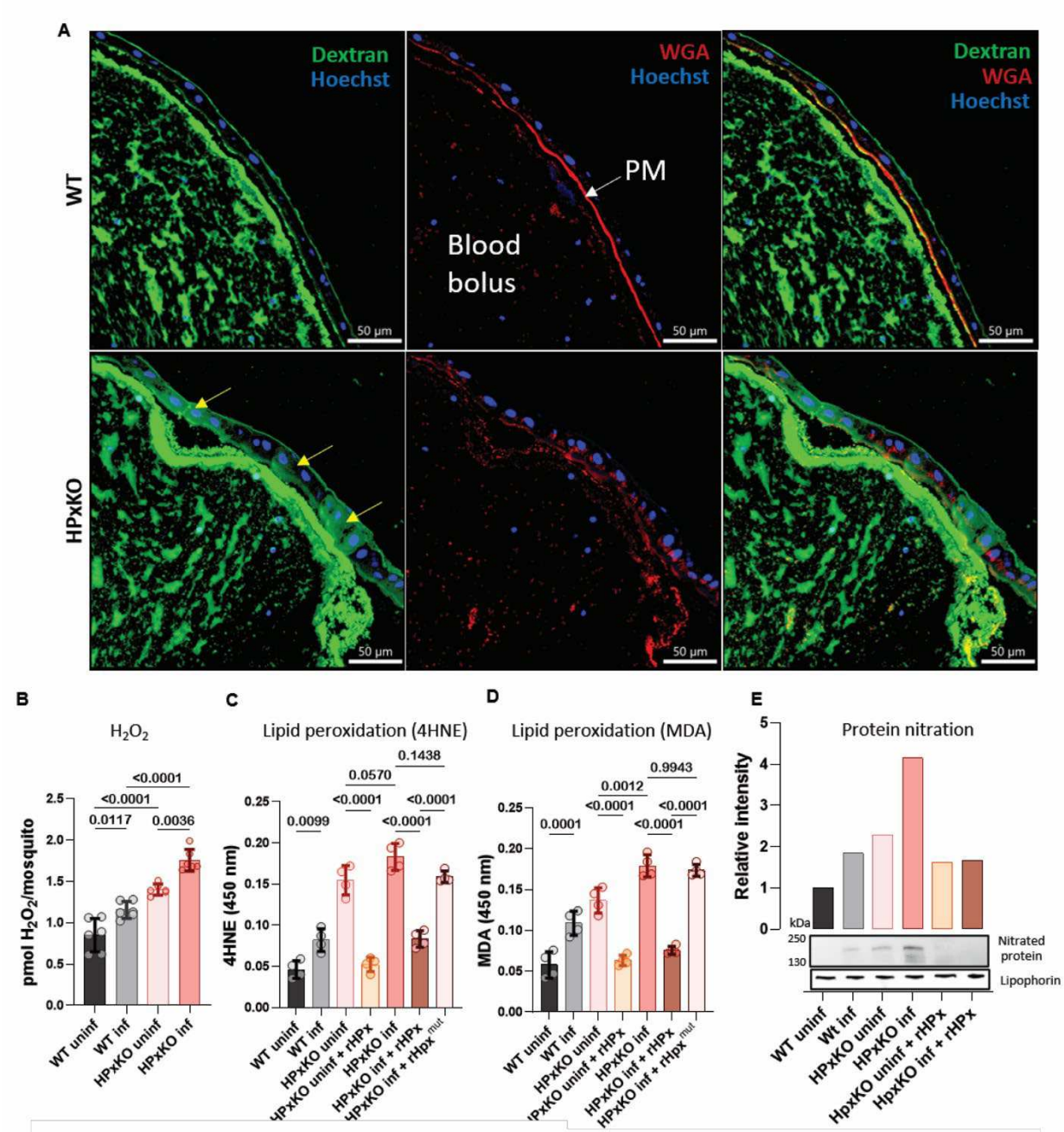
A
WT
HPxKO
Dextran
Hoechst
WGA
Hoechst
Dextran
WGA
Hoechst
PM
Blood
bolus
50 µm
B
H2O2
pmol H2O2/mosquito
C
Lipid peroxidation (4HNE)
4HNE (450 nm)
D
Lipid peroxidation (MDA)
MDA (450 nm)
E
Protein nitration
Relative intensity
kDa
Nitrated protein
Lipophorin
WT uninf
WT inf
HPxKO uninf
HPxKO inf
HPxKO uninf + rHPx
HPxKO inf + rHPx
HPxKO inf + rHPx mut
F
Microbiota load
Relative Expression dCT
WT
HPxKO
n: 22 24
G
48h
96h
Relative Abundance
Ctrl
HPxKO
Yersinia
Serratia
Raoultella
Pseudomonas
Proteus
Prevotella_7
Others
Not_Assigned
Lactococcus
Gluconobacter
Elizabethkingia
Curtobacterium
Corynebacterium
Bifidobacterium
Bacteroides
Asaia
H
(Genus level, 48h; DESeq2)
(Genus level, 96h; DESeq2)
-log10(FDR)
log2(Fold Change)

Figure 4. Hemopexin limits oxidative stress and maintains midgut and microbiota homeostasis. (A) Analysis of midgut barrier integrity 24 h after blood feeding. Mosquitoes were fed blood supplemented with Alexa Fluor 488-conjugated dextran (10 kDa; green), and midguts were stained with wheat germ agglutinin (WGA; red) to visualize the peritrophic matrix (PM). Nuclei were stained with Hoechst (blue). In mosquitoes fed on HPx-KO mice, disruption of the peritrophic matrix (white arrow) was associated with increased diffusion of dextran into epithelial cells (yellow arrows). Representative images from two independent experiments. (B–E) Hemolymph samples were collected from *An. gambiae* mosquitoes 24 h after feeding on uninfected wild-type (WT) or hemopexin-deficient (HPx-KO) mice, or on HPx-KO mice supplemented intravenously with recombinant hemopexin (rHPx) or a heme-binding-deficient mutant protein ($rHPx^{mut}$). Levels of hydrogen peroxide (B), 4-hydroxynonenal (4-HNE) (C), and malondialdehyde (MDA) (D) were quantified as indicators of oxidative damage. Data were pooled from three independent experiments performed in triplicate. Statistical significance was assessed by one-way ANOVA followed by Tukey's multiple-comparison test. (E) Detection of nitrotyrosine, a marker of protein nitration, in mosquito hemolymph by Western blot. Lipophorin was used as a loading control for densitometric quantification. Representative data from two independent experiments are shown. (F) Relative expression of the bacterial 16S rRNA gene in mosquito midguts 24 h after blood feeding, determined by RT-qPCR using universal bacterial primers. Each dot represents an individual midgut. Horizontal bars indicate median values. Statistical significance was determined using the Mann–Whitney test. (G) Relative abundance of the fifteen most abundant bacterial genera in mosquitoes fed on WT or HPx-KO mice at 48 h and 96 h after blood feeding. (H) Differential abundance analysis of bacterial genera at 48 h and 96 h post-blood feeding using DESeq2. Each point represents a bacterial genus. Orange dots represent genera significantly enriched or depleted in HPx-KO-fed mosquitoes (FDR < 0.05), and selected genera are indicated.

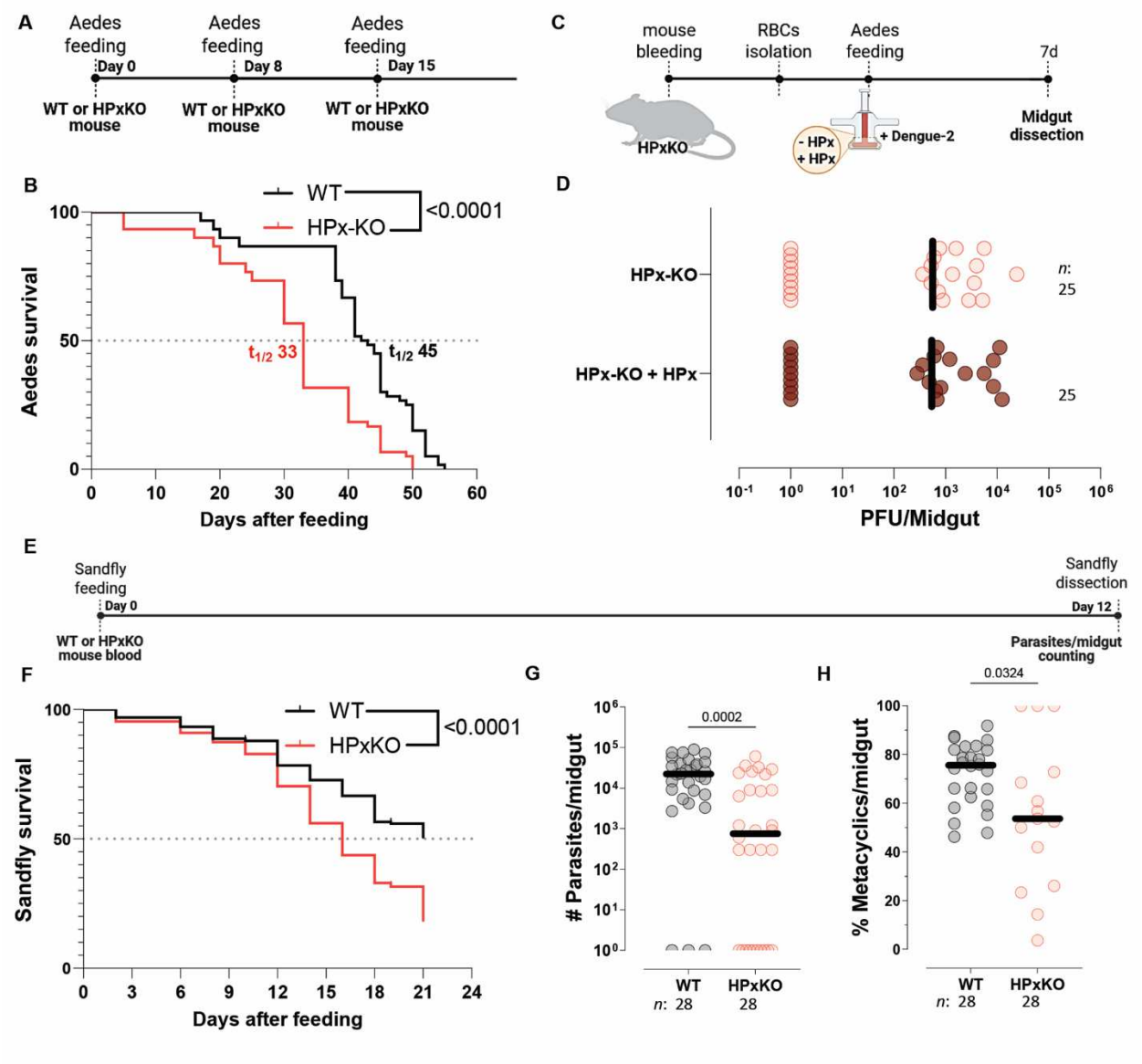

Figure 5. Hemopexin supports dipteran fitness and parasite development across vector systems. (A-B) Experimental design for *Ae. aegypti* survival assays (A). Mosquito survival after feeding on uninfected wild-type (WT) or hemopexin-deficient (HPx-KO) mice on days 0, 8, and 15 (B). Dotted line indicates 50% survival ($t_{1/2}$). Data were pooled from two independent experiments performed in duplicate (n = 30 mosquitoes per assay). Statistical significance was assessed using the log-rank (Mantel–Cox) test. (C-D) Experimental design for dengue virus (DENV-2) infection assays (C). Red blood cells (RBCs) were isolated from HPx-KO mice and mixed with DENV-2 in the presence or absence of recombinant hemopexin (HPx) before membrane feeding to *Ae. aegypti*.

Midguts were dissected 7 days post-infection for viral quantification (D). PFU: plaque-forming units per midgut. Each dot represents one midgut and horizontal bars indicate median values. Data are representative of two independent experiments (n = 25 mosquitoes per group). (E-F) Experimental design for *Leishmania donovani* infections in *L longipalpis* (E). *L. longipalpis* survival after feeding through an artificial membrane on blood containing parasites mixed with blood from WT or HPx-KO mice. and midguts were dissected 12 days later. (F) Survival of sand flies after feeding blood from WT or HPx-KO mice. Representative data from three biological replicates are presented. Statistical significance was assessed using the log-rank (Mantel–Cox) test. (G) Total *L. donovani* parasite burden per sand fly midgut 12 days after infection. Each dot represents one midgut, and horizontal bars indicate median values. (H) Percentage of infectious metacyclic promastigotes in individual infected midguts. Metacyclic frequencies were calculated only from parasite-positive midguts. Data in panels G and H represent pooled results from three biological replicates (n = 28 midguts per group). Statistical significance was determined using the Mann–Whitney test.

SUPPLEMENTARY FIGURES

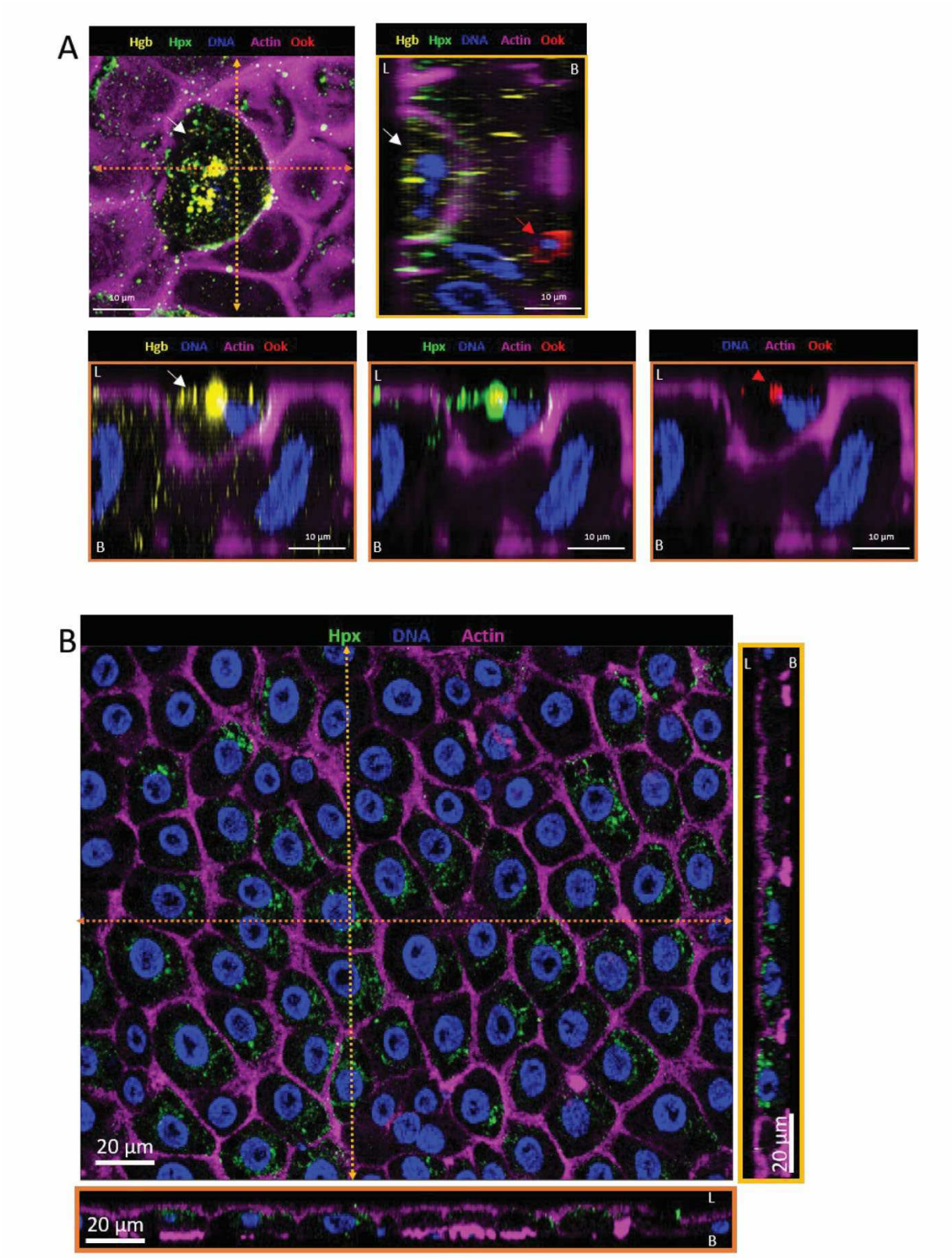

Supplementary Figure 1. Detection of hemopexin and hemoglobin in *P. berghei*-infected midguts. (A) *P. berghei* ookinetes were labeled with a Pbs21 monoclonal antibody (red), and nuclei were labeled with Hoechst (blue). The white arrow points the invaded midgut cells, and the red arrow points the ookinete. (B) Detection of hemopexin inside midgut cells in a region of an infected midgut with no detectable parasites. L: midgut lumen, B: midgut basal side. Colored dotted lines define the *xy* planes.

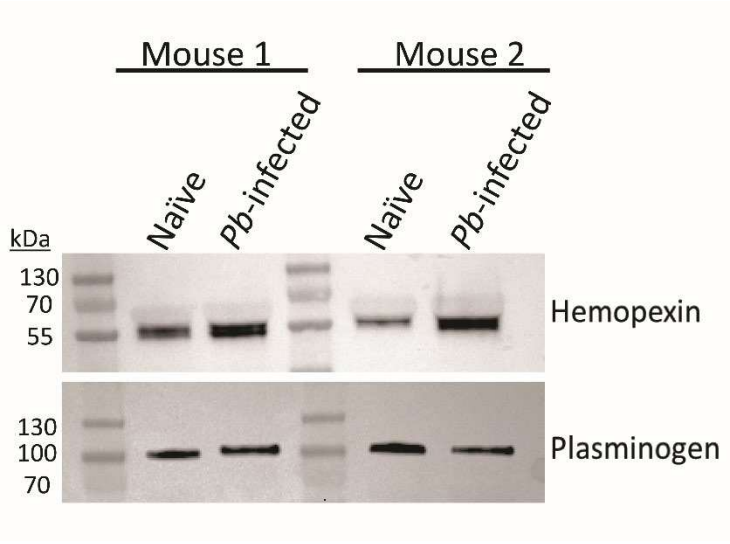

Supplementary Figure 2. Detection of hemopexin in mouse serum following *P. berghei* infection. Serum samples from naïve and *P. berghei*-infected mice were analyzed by Western blot using an anti-hemopexin (HPx) antibody. Plasminogen (Plg) was used as a loading control. Representative blot from three independent experiments.

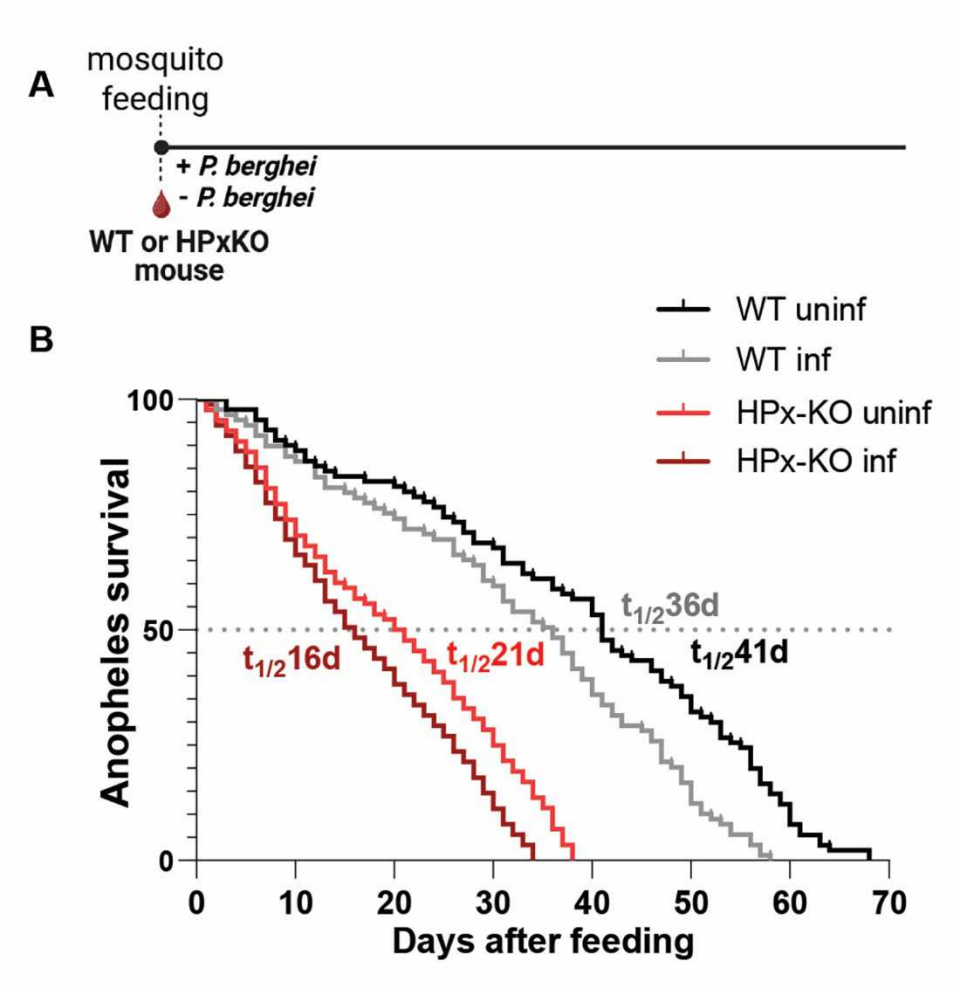

Supplementary Figure 3. Hemopexin contributes to mosquito survival following malaria infection. (A) Experimental design. *An. gambiae* mosquitoes were fed on uninfected wild-type (WT) mice, *P. berghei*-infected WT mice, or *P. berghei*-infected hemopexin-deficient (HPx-KO) mice. (B) Survival of mosquitoes following a single blood meal. Kaplan–Meier survival curves are shown, with the dotted line indicating 50% survival ($t_{1/2}$). Mosquitoes fed on *P. berghei*-infected HPx-KO mice exhibited reduced survival compared with mosquitoes fed on infected WT mice. Data pooled from two independent experiments performed in duplicate (n = 30 mosquitoes per assay). Statistical significance was assessed using the log-rank (Mantel–Cox) test.

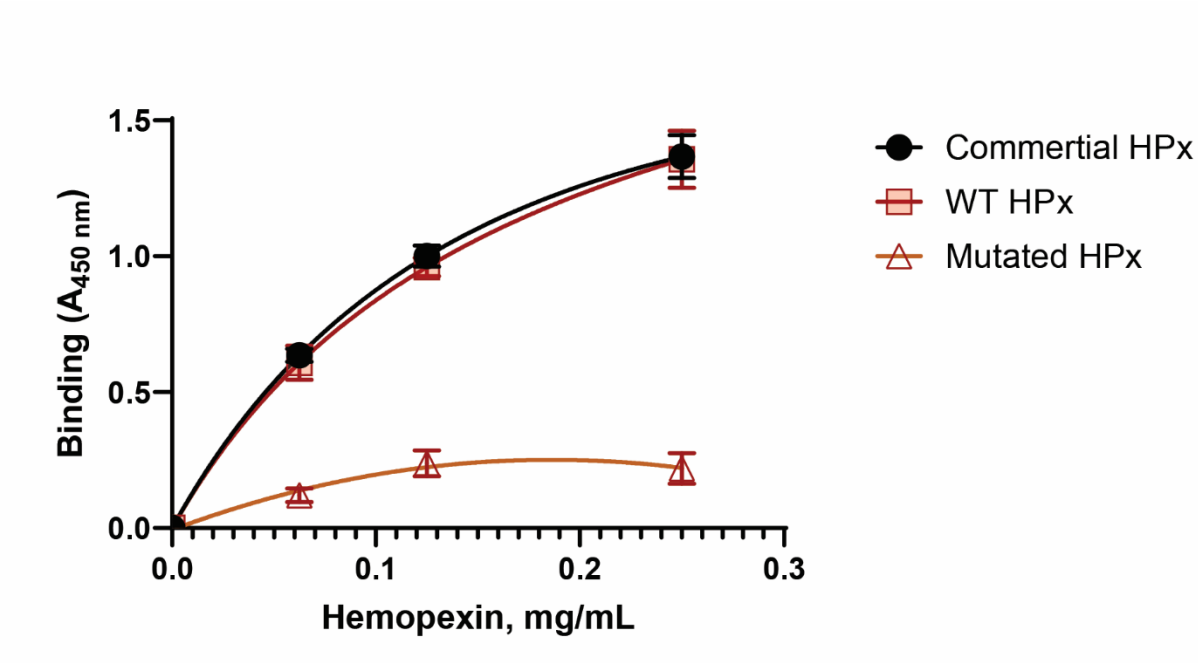

Supplementary Figure 4. Hemopexin–heme interaction assay. Binding of increasing concentrations of commercial human hemopexin, and lab-produced wild-type or mutant recombinant hemopexin, to hemin immobilized in gelatin was quantified using an ELISA-based assay adapted from Bozinovic *et al.* (2020). Hemopexin bound to the hemin gelatin was detected using a mouse anti-hemopexin antibody (SC-373675, Santa Cruz Biotechnology) followed by an HRP-conjugated anti-mouse secondary antibody. Signal was developed with TMB substrate (34028, Sigma).

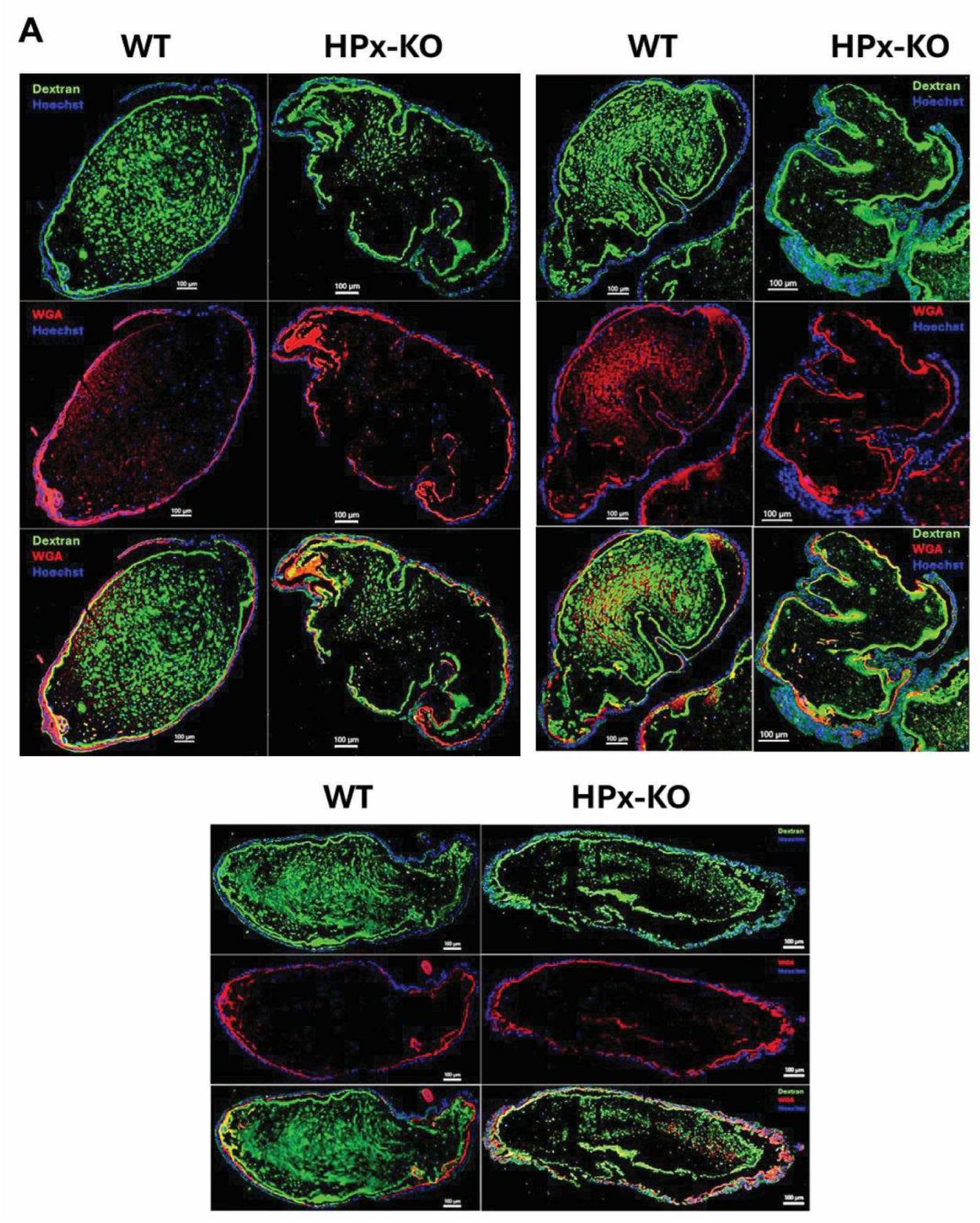
A
WT
HPx-KO
WT
HPx-KO
Dextran
Hoechst
WGA
Hoechst
Dextran
WGA
Hoechst
100 µm
WT
HPx-KO

1077

1078

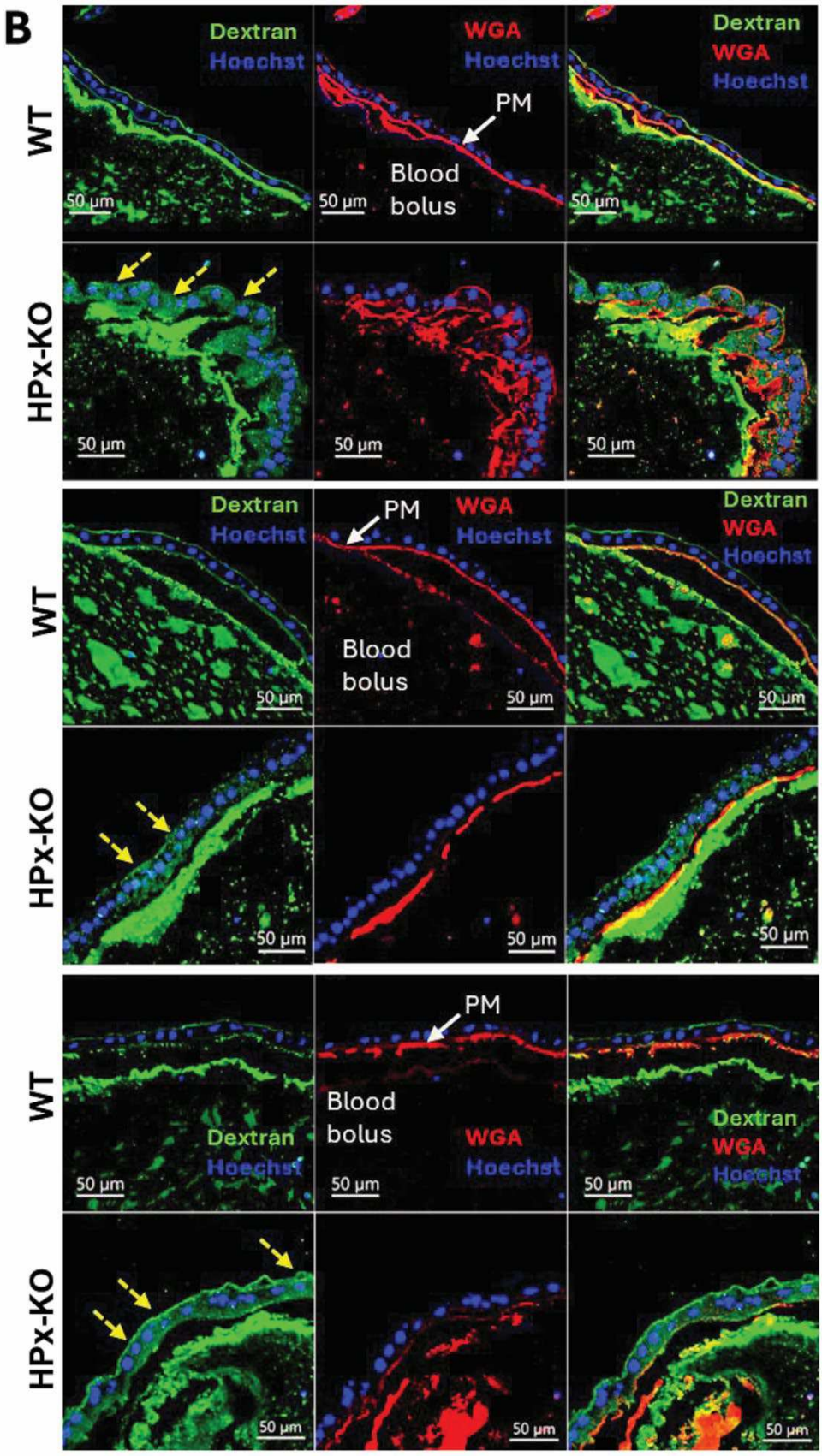
B
WT
HPx-KO
WT
HPx-KO
WT
HPx-KO
Dextran
Hoechst
WGA
Hoechst
Dextran
WGA
Hoechst
PM
Blood
bolus
50 µm

Supplementary Fig. 5. Absence of hemopexin in the blood meal results in peritrophic matrix disruption. Alexa Fluor 488–labeled dextran (10 kDa, green) diffusion into midgut epithelial cells was examined 24 hours after ingestion of dextran-supplemented blood from WT or HPx-KO mice. The peritrophic matrix (PM, white arrows) was visualized by wheat germ agglutinin (WGA) staining (red). (A) Representative whole mosquito midguts images**.** (B) High resolution images of representative areas showing presence or absence of dextran diffusion into the midgut epithelium and peritrophic matrix integrity. Yellow arrows point to dextran diffusion inside the epithelial cells. Scale bars are included in all images.

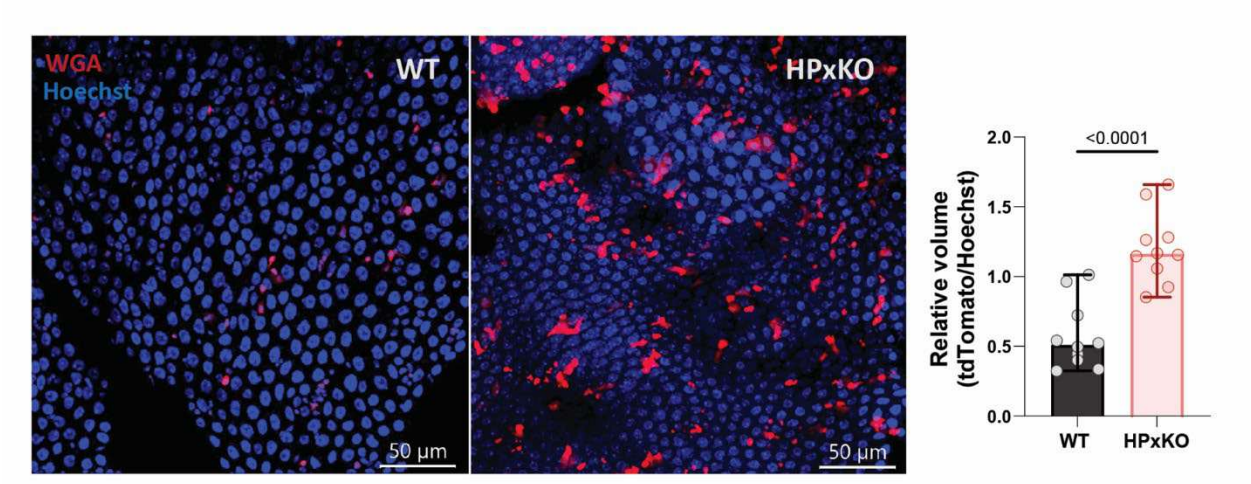

Supplementary Figure 6. Increased midgut damage in mosquitoes fed on hemopexin-deficient mice. Representative confocal images of midguts from *An. stephensi* mosquitoes expressing tdTomato in proliferating midgut stem cells fed on wild-type (WT) or hemopexin-deficient (HPx-KO) mice. Midguts were stained with wheat germ agglutinin (WGA, red) and Hoechst (blue). Quantification of the WGA-positive area is shown on the

right. Data pooled from three independent experiments (n = 10 midguts per group). Statistical significance was determined using an unpaired t-test. Scale bars, 50 μm.

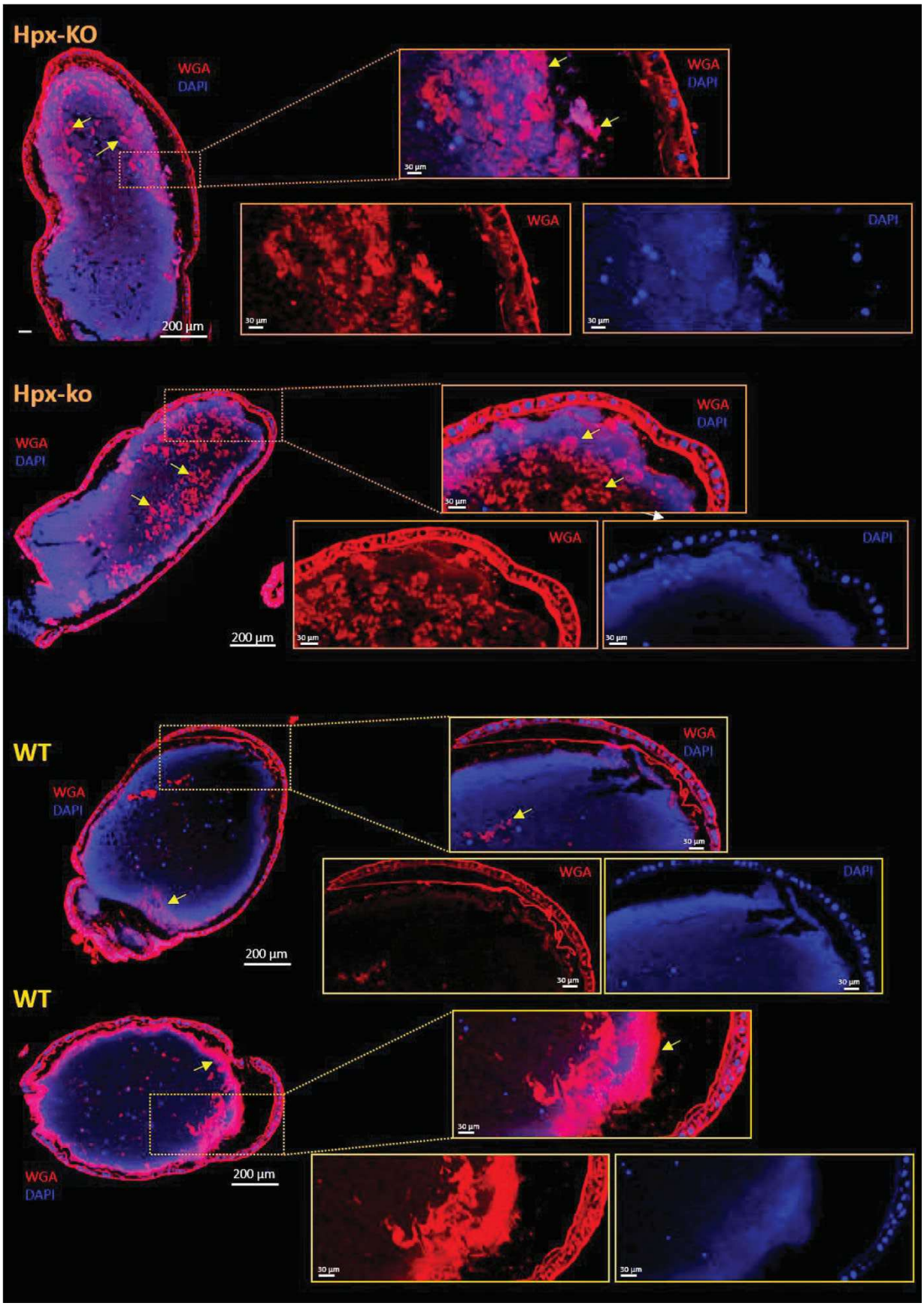
Hpx-KO
WGA
DAPI
200 µm
30 µm
WGA
DAPI
Hpx-ko
WGA
DAPI
200 µm
30 µm
WGA
DAPI
WT
WGA
DAPI
200 µm
30 µm
WGA
DAPI
WT
WGA
DAPI
200 µm
30 µm

1102

Supplementary Fig. 7. WGA staining of mosquito midguts 24 h post–blood feeding. Mosquitoes were fed on wild-type (WT) or hemopexin-deficient (Hpx-KO) mice. Midguts were dissected 24 h after feeding and stained with wheat germ agglutinin (WGA). WGA strongly labels the peritrophic matrix at the periphery of the blood bolus and additionally stains the midgut microbiota within the bolus (yellow arrows). Increased WGA staining is observed in the blood bolus of mosquitoes that fed on Hpx-KO mice compared to those that fed on WT mice.

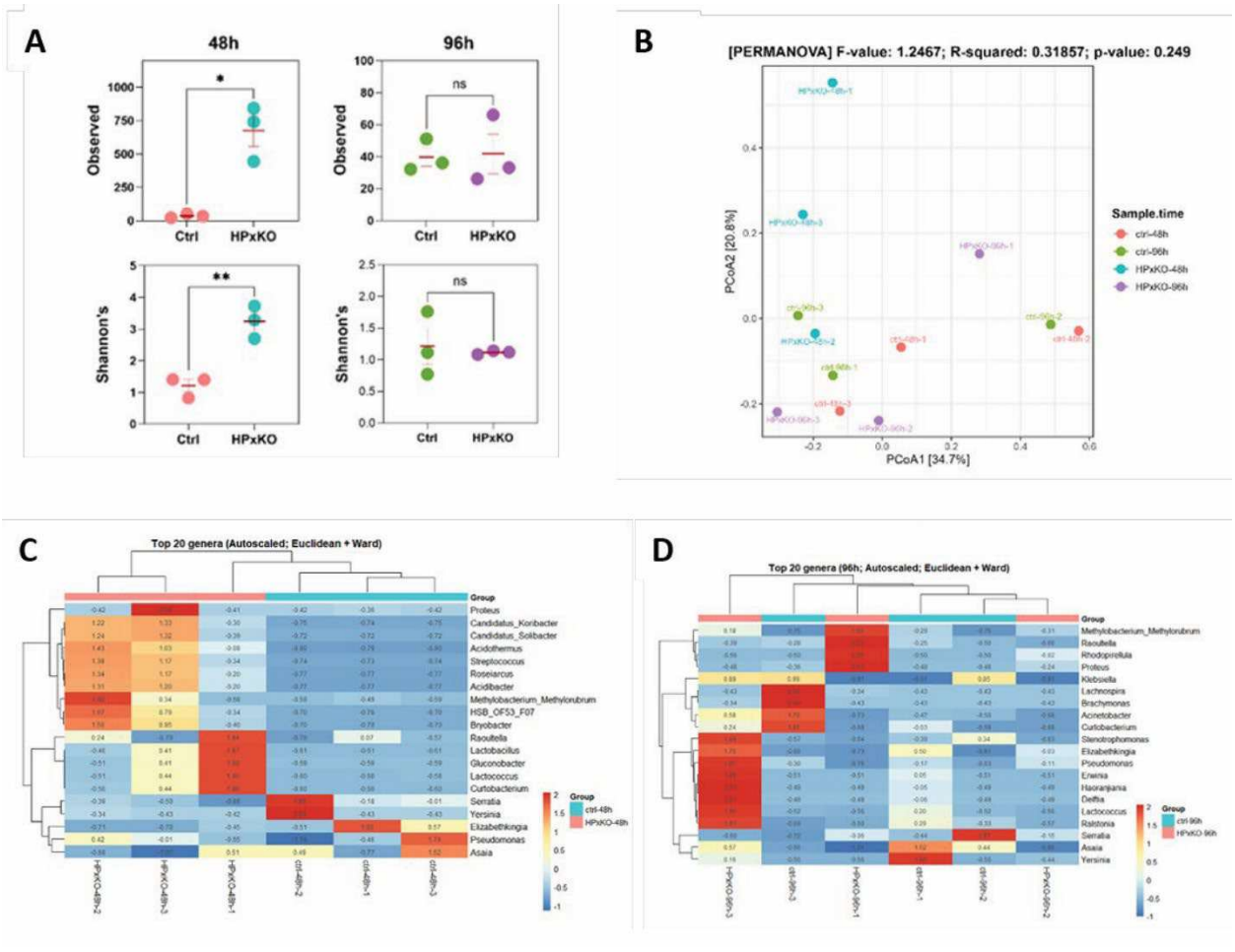

Supplementary Figure 8. Microbiome diversity and taxonomic composition in mosquitoes fed on hemopexin-deficient mice. (A) Alpha diversity analysis of the midgut microbiota at 48 h and 96 h after blood feeding on wild-type (WT) or hemopexin-

deficient (HPx-KO) mice. Richness (Observed taxa) and diversity (Shannon index) are shown for each condition. Statistical significance was assessed using Welch's t-test (*P < 0.05, **P < 0.01; ns, not significant). (B) Principal coordinates analysis (PCoA) based on microbial community composition at 48 h and 96 h post-blood feeding. Each point represents an individual biological replicate. Community structure differences were evaluated using PERMANOVA. (C–D) Hierarchical clustering heatmaps of the 20 most abundant bacterial genera in mosquitoes fed on WT or HPx-KO mice at 48 h (C) and 96 h (D) after blood feeding. Color intensity represents scaled relative abundance values, and clustering was performed using Euclidean distance and Ward's linkage method.

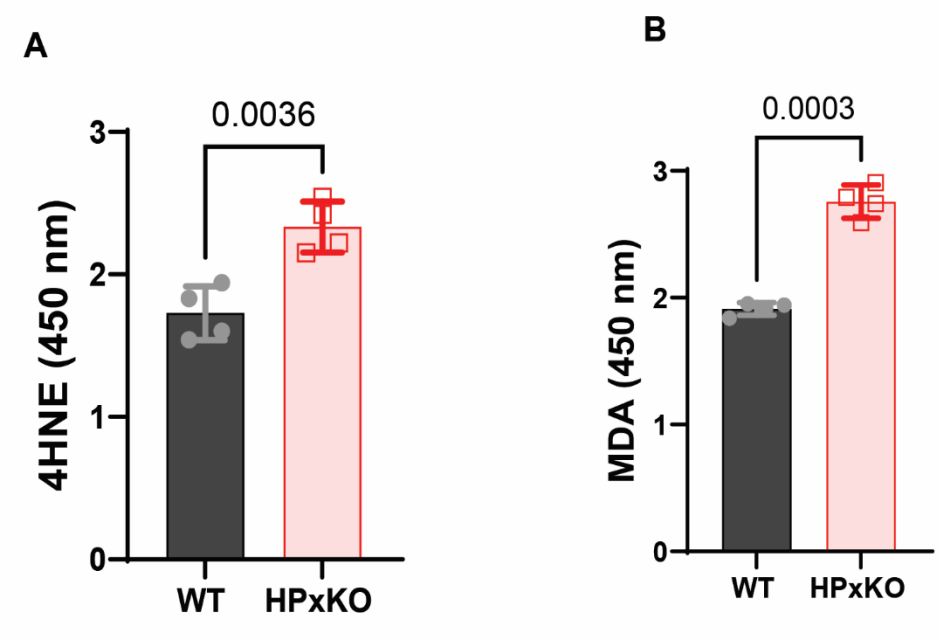

Supplementary Fig. 9. Levels of lipid peroxidation in *Ae. aegypti* hemolymph, assessed by measuring the oxidative stress markers 4-hydroxynonenal (4-HNE) (A) and malondialdehyde (MDA) (B). Quantification was performed using ELISA-based assays. Data pooled from two independent experiments, each conducted in triplicate. Statistical comparisons were performed using unpaired *t*-test, as indicated in the figure.

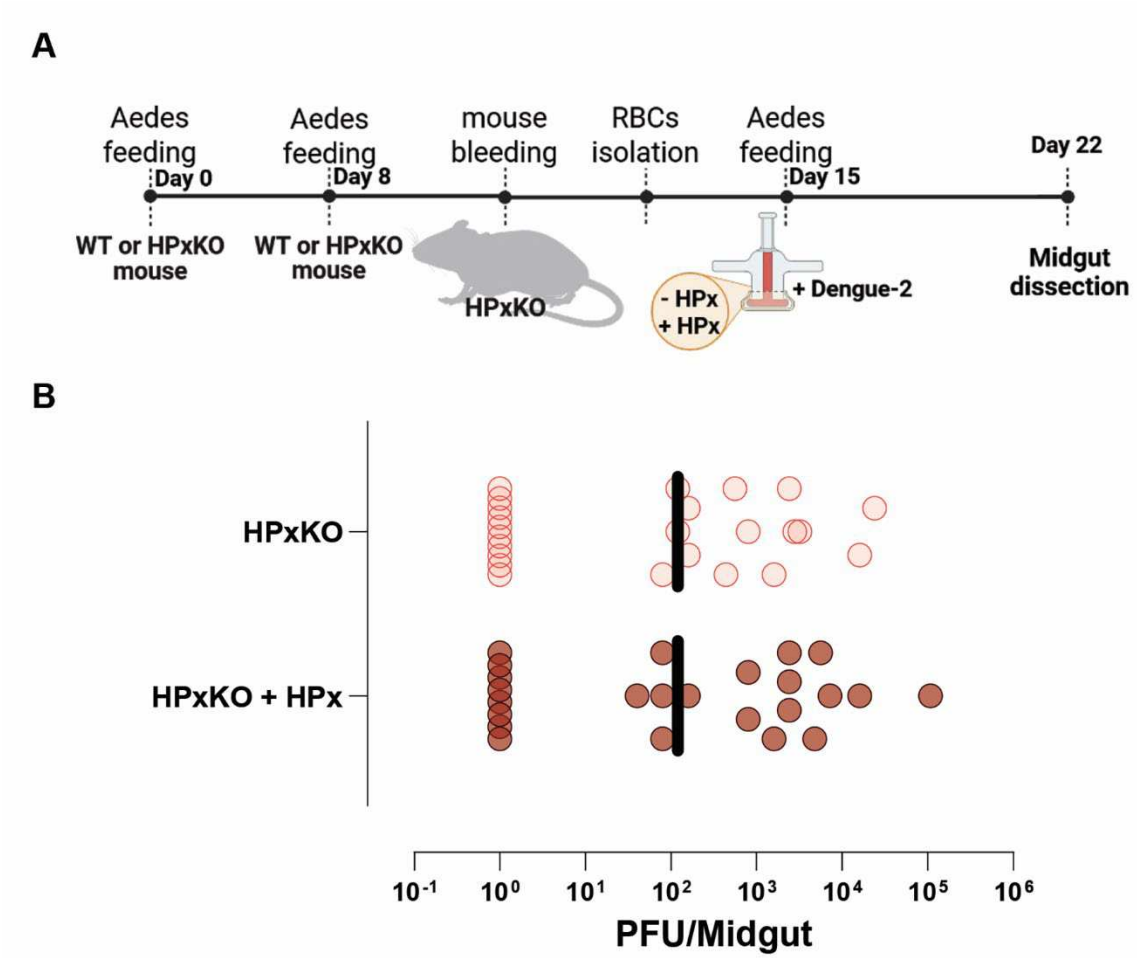

Supplementary Figure 10. Effect of recombinant hemopexin supplementation on dengue virus infection in *Ae. aegypti*. (A) Experimental design. *Ae. aegypti* mosquitoes were fed on wild-type (WT) or hemopexin-deficient (HPx-KO) mice on days 0 and 8. On day 15, red blood cells (RBCs) were isolated from HPx-KO mice and mixed with dengue virus serotype 2 (DENV-2) in the presence or absence of recombinant hemopexin (HPx). Mosquitoes were infected through an artificial membrane feeder, and midguts were dissected 7 days later (day 22) for viral quantification. (B) DENV-2 infection intensity in individual mosquito midguts determined by plaque assay and expressed as plaque-forming units (PFU) per midgut. Each dot represents one mosquito midgut, and black bars indicate median values. Data pooled from two independent experiments (n = 25 mosquitoes per group).

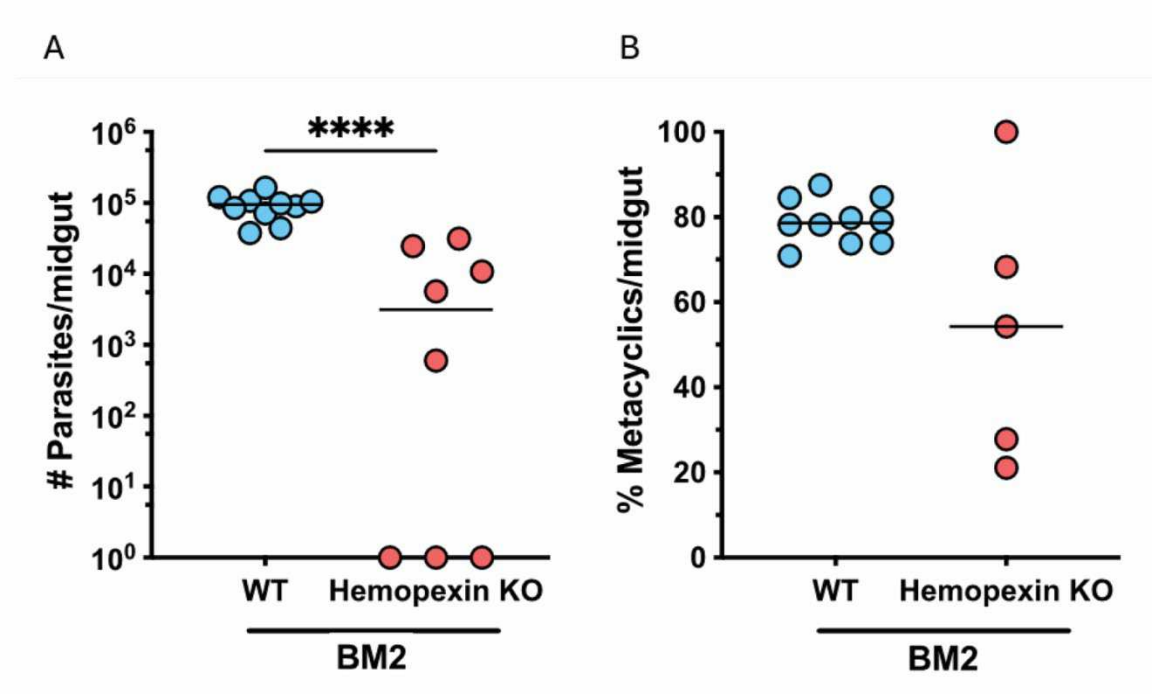

Supplementary figure 11. Long-term detrimental effect of blood from hemopexin knockout mice on *L. donovani* development in sand flies. A-B) At day 21 post-infection, the total parasite load (A) and percent infectious metacyclics (B) per sand fly midgut were assessed in sand flies that took a second uninfected blood meal on day 6 (BM2). The percentage of metacyclic promastigotes was calculated only for midguts positive for parasites (A). Data from one biological experiment, n= 8-10 midguts per group. Statistical analysis by *Mann-Whitney test.* ****P<0.0001.

Supplementary Data Description

Supplementary Data 1. Mouse-derived proteins identified in mosquito hemolymph by label-free proteomics. Mouse proteins detected in cell-free hemolymph from *Anopheles gambiae* mosquitoes fed on uninfected or *Plasmodium berghei*-infected mice. Raw LC-MS/MS data were processed using MaxQuant. Also included are the detected mosquito proteins.

Supplementary Data 2. Differentially expressed genes in mosquito midguts following blood feeding on hemopexin-deficient mice. RNA-seq analysis of *An. gambiae* midguts collected 24 h and 72 h after feeding on wild-type (WT) or hemopexin-deficient (HPx-KO) mice.

Supplementary Data 3. Differentially expressed genes in mosquito carcasses following blood feeding on hemopexin-deficient mice. RNA-seq analysis of mosquito carcasses collected 24 h and 72 h after feeding on WT or HPx-KO mice.

Supplementary Data 4. Differentially expressed genes in mosquito ovaries following blood feeding on hemopexin-deficient mice. RNA-seq analysis of ovaries collected 24 h and 72 h after feeding on WT or HPx-KO mice.

Supplementary Data 5. Functional enrichment analysis of differentially expressed genes in mosquito midguts. Gene Ontology (GO) and pathway enrichment analysis of genes differentially expressed in mosquito midguts following feeding on HPx-KO mice.

Supplementary Data 6. Functional enrichment analysis of differentially expressed genes in mosquito carcasses. Gene Ontology and pathway enrichment analysis of differentially expressed genes identified in mosquito carcasses following feeding on HPx-KO mice. The dataset includes enrichment scores, gene counts, and adjusted p-values.

Supplementary Data 7. Functional enrichment analysis of differentially expressed genes in mosquito ovaries. Gene Ontology and pathway enrichment analysis of differentially expressed genes identified in mosquito ovaries following feeding on HPx-KO mice.

Supplementary Data 8. Single-factor differential abundance analysis at 48 h after feeding. Relative abundance of bacterial genera identified by 16S rRNA sequencing of *An. gambiae* midguts collected 48 h after feeding on WT or HPx-KO mice.

Supplementary Data 9. Single-factor differential abundance analysis at 96 h after feeding. Relative abundance of bacterial genera identified by 16S rRNA sequencing of *An. gambiae* midguts collected 96 h after feeding on WT or HPx-KO mice.

Supplementary Files

This is a list of supplementary files associated with this preprint. Click to download.

- Supplementarydata9.xlsx
- Supplementarydata5.xlsx
- Supplementarydata2.xlsx
- Supplementarydata7.xlsx
- Supplementarydata8.xlsx
- Supplementarydata4.xlsx
- Supplementarydata1.xlsx
- Supplementarydata6.xlsx
- Supplementarydata3.xlsx